# UC San Diego

## UC San Diego Electronic Theses and Dissertations

**Title**

High Magnetic Field Investigations of Correlated Electron Quantum Materials

**Permalink**

https://escholarship.org/uc/item/8nq1p256

**Author**

Breindel, Alexander

**Publication Date**

2021

Peer reviewed|Thesis/dissertation

eScholarship.org Powered by the California Digital Library
University of California

UNIVERSITY OF CALIFORNIA SAN DIEGO

# High Magnetic Field Investigations of Correlated Electron Quantum Materials

A dissertation submitted in partial satisfaction
of the requirements for the degree Doctor of Philosophy

in

Physics

by

Alexander Breindel

Committee in Charge:

Professor Brian Maple, Chair
Professor Daniel Arovas
Professor Richard Averitt
Professor Prabhakar Bandaru
Professor Eric Fullerton

2021

Copyright

Alexander Breindel, 2021

All rights reserved

The dissertation of Alexander Breindel is approved, and it is acceptable in quality and form for publication on microfilm and electronically.

University of California San Diego

2021

# DEDICATION

To my family, my parents, my siblings, for all their love and support through the years.

# EPIGRAPH

It doesn’t matter how beautiful your theory is, it doesn’t matter how smart you are.
If it doesn’t agree with experiment, it’s wrong.

Richard P. Feynman

TABLE OF CONTENTS

LIST OF FIGURES

ACKNOWLEDGEMENTS

I would like to acknowledge Prof. Brian Maple for advising me throughout my doctoral work. His guidance was invaluable in selecting topics of interest and providing support.

I would also like to acknowledge the many other members of the Maple lab over the years whose guidance and help were instrumental in my instruction. Noravee Kanchanavatee, Benjamin White, Duygu Yazici, Colin McElroy, Kevin Huang, Christian Wolowiec, Yuankan Fang, Sheng Ran, Trevor Keiber, Naveen Pouse, Inho Jeon, Sooyoung Jang, Zackary Rehfuss, Kalyan Sasmal, Camilla Moir, and Yuhang Deng.

I would like to acknowledge the help of Prof. Pei-Chun Ho with her assistance, especially with training me on the operation of dilution refrigerators.

I would also like the acknowledge the members of the National High Magnetic Field Laboratory who were of great assistance to me. John Singleton, Marcelo Jaime, and Fedor Balakirev.

I'd like to thank the members of my committee, Prof. Daniel Arovas, Prof. Richard Averitt, Prof. Prabhakar Bandaru, and Prof. Eric Fullerton.

I'd also like to acknowledge the members of UC San Diego staff who were extremely helpful to me, Christine Coffey, Susan Marshall, Mike Rezin, Bradley Hanson, Lester Brooks, Dirk Johnson, and Sharmilla Poddar.

Chapter 3, in full, is currently being prepared for submission for publication of the material. Ran, Sheng; Balakirev, Fedor; Singleton, John; Harima, Hisatomo; Maple, M. Brian. The dissertation author was the primary investigator and author of this material.

Chapter 4, in full, is currently being prepared for submission for publication of the material. Ran, Sheng; Pouse, Naveen; Jeon, Inho; Jaime, Marcelo; Maple, M. Brian. The dissertation author was the primary investigator and author of this material.

Chapter 5, in full, is currently being prepared for submission for publication of the material. Deng, Yuhang; Moir, Camilla; Fang, Yuankan; Lou, Hongbo; Li, Shubin; Zeng, Qiaoshi; Shu, Lei; Wolowiec, Christian; Schuller, Ivan; Rosa, Priscila; Fisk, Zachary; Singleton, John; Maple, M. Brian. The dissertation author was the primary investigator and author of this material.

Finally, I would like to acknowledge the various funding agencies that have contributed to supporting my instruction and my research. I'd like to acknowledge the US Department of Energy Basic Energy Sciences Program for their support through grant No. DE-FG02-04-ER46105, as well as their support for MFMMS experiments through grant No. DE FG02 87ER-45332. I'd like to acknowledge the US National Science Foundation, for their support under grants No. DMR-1206553 and DMR-1810310, as well as their support of the National High Magnetic Field Laboratory under grant No. DMR-1157490/1644779 alongside the State of Florida. I'd like to acknowledge the National Nuclear Security Administration, for their support, under the SSAA program through the US DOE under grant No. DE-NA0002909. This research was also funded by a QuantEmX grant from ICAM and the Gordon and Betty Moore Foundation through Grant GBMF5305 to Alexander Breindel. I'd also like to acknowledge the support of the growth of $SmB_6$ by the US DOE through grant 2019LANLE1FR. I'd like to acknowledge the National Natural Science Foundation of China for their support of DAC measurements through grant No. 51871054. As well as the support of high pressure measurements by the National Key Research and Development Program of China through grants No. 2017YFA0303104 and No.

2016YFA0300503. Lastly, I’d like to acknowledge the financial support of US Naval Information Warfare Center through the San Diego State University Research Foundation under task No. 71-10001

VITA

2013 Bachelor of Science, University of Rochester

2021 Doctor of Philosophy, University of California San Diego

PUBLICATIONS

Alexander Breindel, Diankang Sun, and Surajit Sen, “Impulse absorption using small, hard panels of embedded cylinders with granular alignments,” *Applied Physics Letters* **99**, 063510 (2011), DOI: http://dx.doi.org/10.1063/1.3624466

A. J. Breindel, R. E. Stuart, W. J. Bock, D. N. Stelter, S. M. Kravec, and E. M. Conwell, “Hole Wave Functions and Transport with Deazaadenines Replacing Adenines in DNA,” *The Journal of Physical Chemistry B* **117,** 3086-3090, (2013) DOI: http://dx.doi.org/10.1021/jp310636k

B. D. White, D. Yazici, P-C. Ho, N. Kanchanavatee, N. Pouse, Y. Fang, A. J. Breindel, A. J. Friedman, and M. B. Maple, "Weak hybridization and isolated localized magnetic moments in the compounds $CeT_2Cd_{20}$ (T = Ni, Pd)," *Journal of Physics: Condensed Matter* **27**, 315602 (2015). DOI: http://dx.doi.org/10.1088/0953-8984/27/31/315602

Nicholas P. Butch, Sheng Ran, Inho Jeon, Noravee Kanchanavatee, Kevin Huang, Alexander Breindel, M. Brian Maple, Ryan L. Stillwell, Yang Zhao, Leland Harriger, and Jeffrey W. Lynn, “Distinct magnetic spectra in the hidden order and antiferromagnetic phases in $URu_{2-x}Fe_xSi_2$,” *Phys. Rev. B* **94**, 201102 (2016). DOI: https://doi.org/10.1103/PhysRevB.94.201102

Sheng Ran, Inho Jeon, Naveen Pouse, Alexander J. Breindel, Noravee Kanchanavatee, Kevin Huang, Andrew Gallagher, Kuan-Wen Chen, David Graf, Ryan E. Baumbach, John Singleton and M. Brian Maple, “Phase diagram of $URu_{2-x}Fe_xSi_2$ in high magnetic fields,” *PNAS* **114**, 9826-9831 (2017). DOI: https://doi.org/10.1073/pnas.1710192114

Y. Fang, C. T. Wolowiec, A. J. Breindel, D. Yazici, P.-C. Ho, and M. B. Maple, “Upper Critical magnetic Field of $LnO_{0.5}F_{0.5}BiS_2$ (*Ln* = La, Nd) superconductors at ambient and high pressure,” *Supercond. Sci. Technol.* **30,** 115004 (2017). DOI: https://doi.org/10.1088/1361-6668/aa8829

I. Jeon, S. Ran, A. J. Breindel, P.-C. Ho, R. B. Adhikari, C. C. Almasan, B. Luong, and M. B. Maple, “Crossover and coexistence of superconductivity and antiferromagnetism in the filled-skutterudite system $Pr_{1-x}Eu_xPt_4Ge_{12}$,” *Phys. Rev. B* **95,** 134517 (2017). DOI: https://doi.org/10.1103/PhysRevB.95.134517

K. Huang, D. Yazici, B. D. White, I. Jeon, A. J. Breindel, N. Pouse, and M. B. Maple, “Superconducting and normal state properties of the systems $La_{1-x}M_xPt_4Ge_{12}$ (*M* = Ce, Th),” *Phys. Rev. B* **94,** 094501 (2016). DOI: https://doi.org/10.1103/PhysRevB.94.094501

Yinming Shao, Zhiyuan Sun, Ying Wang, Chenchao Xu, Raman Sankar, Alexander J. Breindel, Chao Cao, Michael M. Fogler, Andrew J. Millis, Fangcheng Chou, Zhiqiang Li, Thomas Timusk, M. Brian Maple, and D. N. Basov, “Optical signatures of Dirac nodal lines in $NbAs_2$,” *PNAS* **116**, 1168-1173 (2018). DOI: https://doi.org/10.1073/pnas.1809631115

Christian T. Wolowiec, Noravee Kanchanavatee, Kevin Huang, Sheng Ran, Alexander J. Breindel, Naveen Pouse, Kalyan Sasmal, Ryan E. Baumbach, Greta Chappell, Peter S. Riseborough, and M. Brian Maple, "Isoelectronic perturbations to f-d-electron hybridization and the enhancement of hidden order in $URu_2Si_2$," *PNAS* **118.20**, (2021). DOI: https://doi.org/10.1073/pnas.2026591118

ABSTRACT OF THE DISSERTATION

High Magnetic Field Investigations of Correlated Electron Quantum Materials

by

Alexander Breindel

Doctor of Philosophy in Physics

University of California San Diego, 2021

Professor M. Brian Maple, Chair

This dissertation goes over the results of high magnetic field and other measurements on various correlated electron quantum materials. These measurements include Shubnikov de Haas quantum oscillations measurements as a function of angle for $PrT_2Cd_{20}$ (T = Ni, Pd). Such

measurements allow investigation of the heavy Fermion behavior in these systems as well as probing the shape of the Fermi surface. Other measurements include high field magnetostriction measurements of $URu_{2-x}Fe_xSi_2$. $URu_2Si_2$ is a compound which exhibits a mysterious hidden order phase, and Fe doping has been shown to enhance this hidden order behavior. The magnetostriction measurements allow the further investigation of the associated high field, doped, phase diagram of this material, including indicating interesting phase transitions and also opens the possibility of investigating the development of the antiferromagnetic order in the compound. Lastly, $SmB_6$ and FeSi are compared along various lines of measurement, including high field resistivity, resistivity under pressure, and Magnetic Field Modulated Microwave Spectroscopy (MFMMS). This comparison shows several similarities in the results of these measurements between these compounds, which are both suggested as possible topological Kondo insulators. However, there are also clear differences in the MFMMS result, suggesting the possibility that the surface physics of the compounds may be different.

## Chapter 1: Introduction

Magnetic fields and their impact upon materials has been the subject of experimental investigation since Pierre de Maricourt's Letter on the Magnet in 1269 [1]. Although poorly understood at first, electromagnetism is now understood as being among four fundamental forces in physics, and its use has become ubiquitous in the modern world [2]. Much of the technological advancement of the last centuries has been due to our increasing understanding of how electromagnetism interacts with various materials. Magnetic fields can now be used to investigate a variety of different properties of materials, such as phase transitions and ground state Fermi surface analysis.

Over the past few decades higher fields have been able to be more reliably achieved allowing their use in investigating materials to become more accessible. For example, the National High Magnetic Field Laboratory is now able to achieve pulsed fields up to 300 T using a single turn magnet [3]. These high magnetic fields can be used to explore the phase space of materials, as high fields may induce materials into new phases of matter. Another example where high fields can be useful is in inducing quantum oscillations in highly correlated materials which can exhibit heavy effective Fermion masses [4]. Quantum oscillations, as will be discussed later, can be used to analyze their Fermi surface, which is important in determining their physical properties. Large masses require higher fields to perform quantum oscillations measurements [4].

In addition to achieving higher and higher magnetic fields, new magnetic field techniques are being developed to probe material properties, by using oscillating fields or electromagnetic waves. One such new technique is Magnetic Field Modulated Microwave Spectroscopy

(MFMMS) [5]. This technique, which will be discussed in greater detail later, utilizes oscillating fields to probe changes in the surface absorption of materials to probe for phase transitions [5].

**Outline of Dissertation**

This introduction gave a very brief history of magnetic fields and some of their applications in studying materials in physics research. Newer techniques, which will be relevant in subsequent chapters, were also discussed. The following chapter will lay down some background knowledge, with a focus on laboratory experimental techniques needed in the course of the research that lead to this thesis. Chapters 3, 4, 5 will be research being prepared for publication involving the research of particular materials using these and other techniques. Each of the research projects covered by these chapters involved the use of pulsed, high magnetic fields. Chapter 3 will cover research on quantum oscillations in the strongly correlated system $PrT_2Cd_{20}$ (T = Pd, Ni). Chapter 4 will go over research on magnetorstriction measurements of $URu_{2-x}Fe_xSi_2$. Chapter 5 will go over research comparing FeSi and $SmB_6$ in various ways including MFMMS and high field resistance measurements.

**Bibliography**


1. David Wootton. “The Invention of Science: A New History of the Scientific Revolution” **First US Edition** Harper Collins (2015) ISBN 978-0-06-175952-9

2. David J. Griffiths. “Introduction to Electrodynamics” **3** Pearson Addison-Wesley (1999) ISBN 0-13-805326-X

3. M. Jaime, A. Lacerda, Y. Takano, and G. S. Boebinger. “The National High Magnetic Field Laboratory.” *Journal of Physics: Conference Series*, **51** 643-646 (2006). DOI: https://doi.org/10.1088/1742-6596/51/1/148

4. Charles Kittel. “Introduction to Solid State Physics” **8** John Wiley & Sons, Inc (2005) ISBN 978-0-471-41526-8

5. Juan Gabriel Ramírez, Ali C. Basaran, J. de la Venta, Juan Pereiro, and Ivan K. Schuller. “Magnetic Field Modulated Microwave Spectroscopy Across Phase Transitions and the Search for New Superconductors.” *Reports on Progress in Physics*, **77** 093902, (2014). DOI: http://dx.doi.org/10.1088/0034-4885/77/9/093902

## Chapter 2: Background: Theory and Experiment

Crystals produced in a lab can be broadly divided into two categories, polycrystals and single crystals. This distinction refers to whether the entire crystal structure at the atomic level is oriented in the same direction or not. A single crystal (ideally) has its entire crystal structure uniform throughout, whereas a polycrystal can be thought of as many small single crystals arranged in haphazard direction to one another.

Many methods exist for producing crystals, and the method used must fit the desired growth. One method, flux growth, involves growing the crystal inside of a molten flux, typically made of one of the constituents of the crystal [1]. For instance, $PrNi_2Cd_{20}$ crystals may be grown in a cadmium (Cd) flux. This method is similar to solution growth methods that are done at lower temperatures, like the methods that are used in home demos for making rock candy or salt crystals. In these solution growth methods, crystals form by saturating in a solvent. However, the flux method differs in that heat transport determines the rate of crystal growth instead of the coupling of mass transport of the molecules in the solution and integration of molecules at the crystal surface [2]. In the flux method, the constituents are dissolved in the molten flux, and the crystal forms within, as the temperature is lowered [1]. A common disadvantage when using flux growths is that it tends to produce small crystals [1].

Another important method for crystal growth is the Czochralski method. This method was discovered by mistake; in 1916 Jan Czochralski accidentally dipped his pen into molten tin rather than into an inkwell [3]. Withdrawing his pen resulted in a single crystal of tin [3]. This method is used to produce nearly all the high purity semiconductor silicon used in the integrated circuits that show up in various electronics [3]. The technique involves using a pulling rod,

sometimes with a seed crystal, and using it to pull crystal out of a molten material [4]. As the crystal is lifted it cools and the constituents are encouraged form in line with the cooler crystal above, resulting in very large single crystals [4]. Different techniques are used to create the molten melt. For instance, one might use resistive heating to create a melt in a crucible, or one might use an arc furnace with electrical arcs [4, 5].

Once a crystal is grown, it is often useful to check that the correct crystal structure formed and also sometimes necessary to orient the crystal. Crystals form in a variety of different structures, which may be anisotropic. It is frequently not apparent, from the macroscopic properties of the crystal, the actual orientation of such an anisotropic crystal lattice. Various pieces of information can help inform on the orientation, such as knowledge of crystal axes where the structure might cleaves easily. However, to orient the crystal fully, one frequently has to turn to experimental techniques capable of probing the crystal lattice. This is often done with x-ray techniques, where the scattering of x-rays off of the crystal lattice is used to determine the crystal structure properties of the sample, such as the lattice spacing or the orientation [6]. One technique that is particularly helpful for determining orientation of samples is Laue diffraction [6]. Here, the diffraction of incoming x-rays either transmitted through the crystal or in back scattered off of it produce a dot pattern, called a Laue pattern, which can be used to determine the orientation of the crystal. This determination is done through a series of equations called Laue equations, which describe what such a dot pattern would look like for a particular incoming x-ray wave on a particular crystal structure in a particular orientation. These equations have helpfully been modeled by various computer programs, which aid in matching data taken using x-ray imaging devices.

In a similar manner to the Laue technique, a powder x-ray diffraction technique is used to verify the crystal formed the correct structure. This is done by turning some of the crystals into a powder through grinding, and then x-rays reflected off the powder are analyzed based on the angle of scattering, the powder is assumed to be oriented randomly, which allows every angle to be probed simultaneously, the peaks in the x-ray detection can be matched against databases and theoretical calculations to determine the lattice parameters and crystal structure of the crystal [6].

Low temperatures are a ubiquitous and crucial part of current condensed matter research. By driving systems to low temperatures, energetic fluctuations are suppressed, allowing more interesting quantum mechanical effects to dominate the behavior of the system. This sees application most prominently in superconductors, the maximum temperature of which has been driven higher and higher in recent years, with room temperature superconductivity having recently been achieved, albeit at high pressures, such as yittrium superhydride which has a critical temperature of 262 K at 182 GPa [7]. Commercial superconductors are often used in medical MRI machines, which are cooled using liquid helium [8]. This is done in the same evaporative manner as is often done with water cooling, such as is used when one sprays oneself with a water bottle on a hot day. However, helium is liquid at a much lower temperature, at 4.2 K, allowing access to these lower temperatures for the MRI superconductors.

In order to go below 4.2 K, one can pump on a liquid helium bath. This lowers the boiling point, due to lower pressure, and drives the temperature to around 1 K. To go lower still a pure bath of the isotope Helium 3 can achieve temperatures of 3.19 K at atmospheric pressure, and when pumped can typically achieve temperatures of 0.3K [9]. The extremely high cost of helium 3 encourages its use almost exclusively in systems where the gas can be recovered and reused.

Lower temperatures than this are typically achieved using a device called a dilution refrigerator. This device is capable of reaching temperatures of as low as 2 mK [10], although between 10 and 50 mK is more typical. This is done by circulating a mixture of He3 and He4, which, at a specific temperature, endothermically phase separates into He3 dilute and rich mixture. Heat exchangers are used to reinforce this cooling cycle, using the circulating mixture to cool itself and continuously drive the temperature lower until the heat exchangers can no longer efficiently cool the system [10].

It is clear that these processes are heavily dependent on the use of Helium, which is an increasingly valuable resource, as it becomes more scarce and more and more useful applications are discovered. This has encouraged movement away from these comparatively simpler methods which consume large amounts of helium towards more complex, but less helium intensive, methods for reaching low temperatures. Temperatures of around 1 K can be achieved using a device called a pulse tube cryocooler, which allows a pressurized gas to cool to a lower temperature before depressurizing it, taking advantage of the same cooling power that a compressed air can produces to reach lower temperatures [10]. This is the method used in the widespread commercial DynaCool Physical Property Measurement System [11]. This system has become widespread in the condensed matter community to continue to perform low temperature research as resources become scarce.

A typical way of achieving significant magnetic fields in a research laboratory is the use of superconducting magnets. These magnets are made of superconducting material. Because of the properties of superconductors, a current in a loop of this material does not decay (experimental observation has put the time constant for the current decay at over 100,000 years [12]). This can thus be used to set up a persistent magnetic field. Superconducting magnets need

to be kept at low temperatures to maintain their properties. Typical commercial magnets used in research labs can often generate fields of around 9 T.

Superconducting magnets can be used to generate high fields, commonly around 3-20T, although some can generate up to 40T. To get even higher fields one has to use pulsed magnetic fields. This is done using a large current generated from a large number of capacitors. The current is sent through a copper coil which is cooled through liquid nitrogen, which can generate fields up to 60T. These pulsed high magnetic fields are generated at the National High Magnetic Field Laboratory at Los Alamos National Laboratory.

Magnetostriction measures the change in the physical size of the sample in response to an applied field. For very high, pulsed, field measurements, these measurements must be performed suitably rapidly. This is done by using an optical fiber with an embedded Bragg grating. The sample is attached to the fiber using GE varnish. When the sample expands or contracts, the grating is distorted, and this distortion changes how the light is reflected back along the fiber. Thus, one can use the distortion to realize the change in shape of the sample. [13]

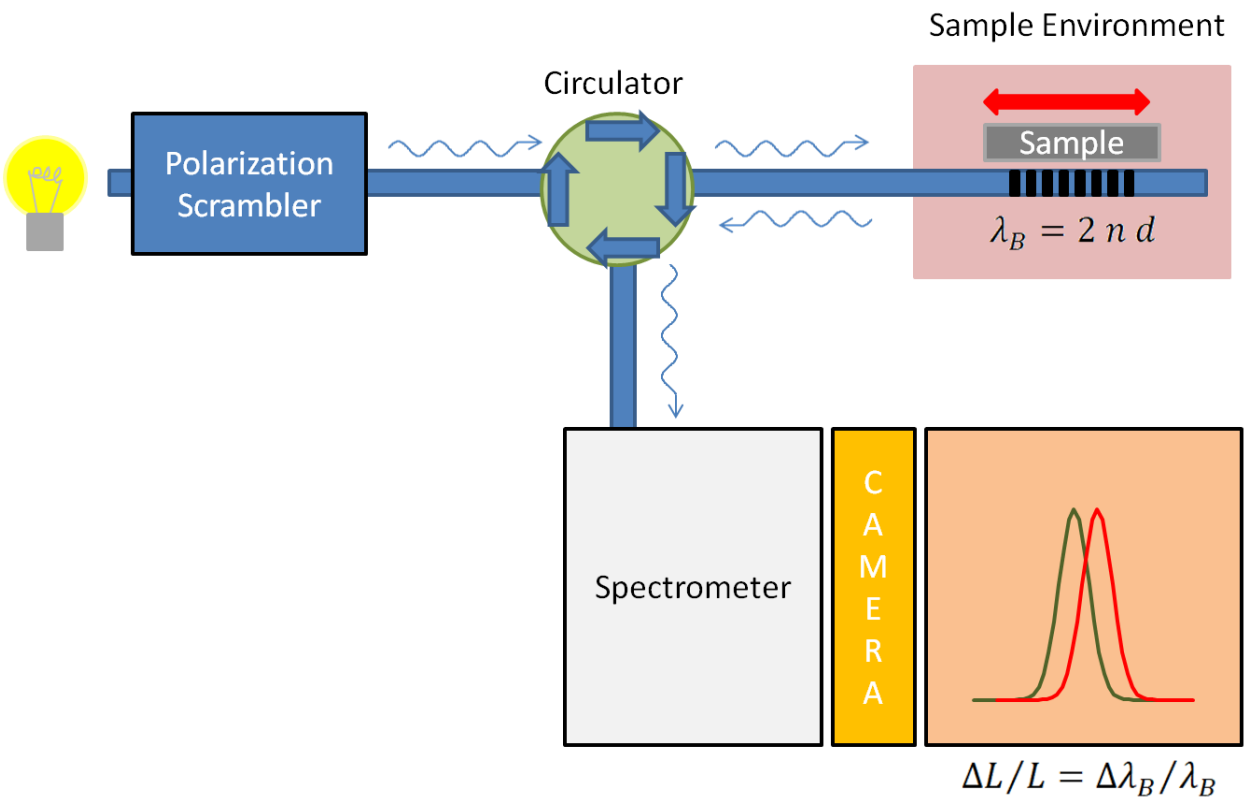


**Figure 2-1** Diagram (based on ref. [13]) showing the setup for a magnetostriction experiment. Broadband light in the 1500 to 1600 nm range is sent down a optical fiber. A band of this light around 1550 nm is reflected by the Bragg grating. The actual wavelength that is reflected is determined by the spacing of the grating, which changes along with the length of the sample. A circulator diverts the reflected light to a spectrometer for recording and analysis [13].

The setup for this is shown in the figure 2-1. A superluminescent light emitting diode or SLED is used to generate a broadband white light in the 1500 to 1600 nm range. A band of this light around 1550 nm is reflected by the Bragg grating. The actual wavelength around which the light is reflected is determined by the spacing of the grating, which changes along with the length of the sample attached to the fiber. This is given by $\lambda_B = 2\,n\,d$, where $n$ is the index of diffraction of the fiber and $d$ is the spacing of the grating. A circulator is used to divert the reflected light to a spectrometer for recording and analysis.

The Shubnikov de Haas effect refers to small oscillations in the resistivity of a material in response to a magnetic field. These oscillations correspond to changes in the density of states at the Fermi surface, which impact the scattering probability. Thus these oscillations can be used to probe the Fermi surface. In the high, pulsed, magnetic fields, a proximity detector oscillator (PDO) circuit is used to measure the conductivity by using the changes in an LC circuit where there is a coil wrapped around the sample [14]. Changes in the surface conductivity impact the inductance of the coil, allowing them to be measured.

Following a method outlined by Kittel [15] we can explain the formation of these oscillations as the result of the rearrangement of electron orbitals in reciprocal (momentum) space in the presence of a magnetic field. In a simple 2 dimensional model, available quantized electron states can be imagined as a grid as shown on the left of figure 2-2

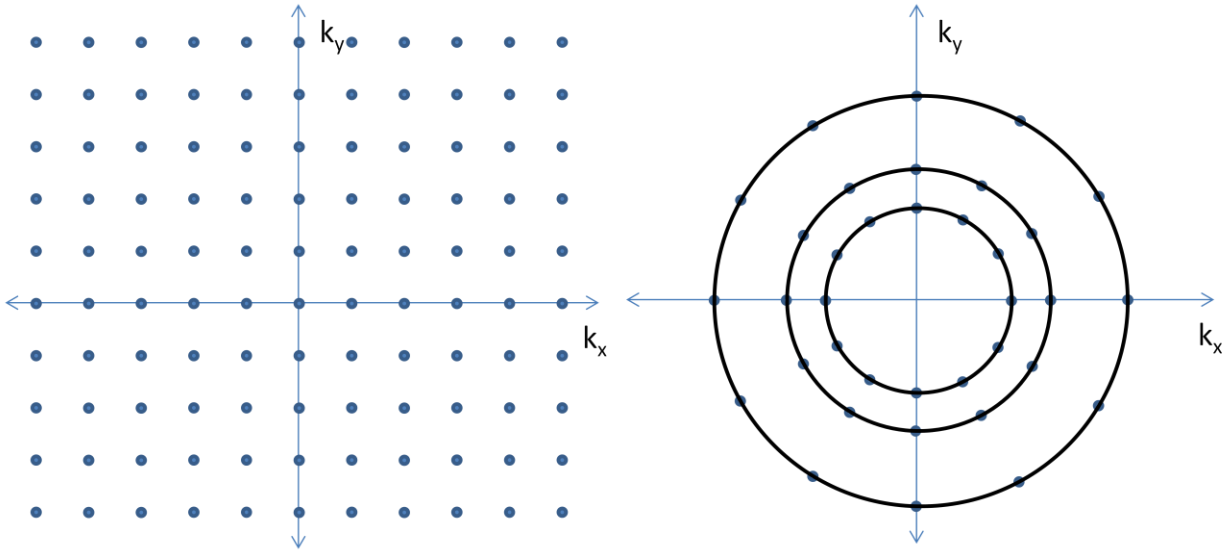


**Figure 2-2** Simple 2D model of quantized electron states, shown in reciprocal space (left) in absence of a magnetic field (right) in the presence of a magnetic field. In the presence of the field, the states arrange themselves into circular Landau levels.

the points on the grid correspond to available momentum values the electrons can take on while still obeying Pauli exclusion rules.

A simple formula to describe an electron's motion in a magnetic field can be given by:

$$\vec{F} = \frac{-e}{c}\vec{v} \times \vec{B}$$

where v is velocity, e is the electron charge, c is the speed of light, B is a magnetic field, F is the force experienced by the electron. If we want to relate this to momentum space, we can use $\vec{F} = \frac{d\vec{p}}{dt}$ and $\vec{p} = \hbar\vec{k}$, which, along with some simple manipulations gets us the equation

$$r^2 = (\frac{c\hbar}{eB})^2 k^2$$

This equation allows us to relate the real space area A with the reciprocal space area S

$$A = (\frac{c\hbar}{eB})^2 S$$

We now call upon the well established quantization of magnetic flux, where the formula for a quanta of magnetic flux is given by

$$\Phi = BA = n\frac{2\pi\hbar c}{e}$$

This allows us to relate the quantization within a magnetic field to the real space area, so taking the two equations together allows us to see the reciprocal space area must be arranged in quantized levels

$$S_n = n\frac{2\pi e}{\hbar c}B$$

These quantized levels are called Landau Levels. They can be seen on the right of figure 2-2. The number of electron orbitals that are in each Landau level can be given by D:

$$D = \frac{S_{n+1} - S_n}{S_{free}} = \xi B$$

Where $S_{free}$ represents the density of orbitals in reciprocal space in absence of the magnetic field. The reason this equation works is because the orbitals are conserved, they've rearranged themselves in the presence of the magnetic field. $\xi = \frac{2\pi e}{\hbar c S_{free}}$ is a term collecting the constants, in order to show that D is directly proportional to B.

To see the oscillations, we consider the situation at the Fermi surface. The Fermi surface is at the Fermi energy, where the last occupied electron orbital is, so the number of empty states there, for a number of filled orbitals N is going to be given by

$$\Delta D_{states}(E_F) = \eta D - N$$

where $\eta$ represents the index of the last filled orbital. This index can be related to D and N via the ceiling function: $\eta = \left\lceil \frac{N}{D} \right\rceil$, so we can rewrite this in terms of B as

$$\Delta D_{states}(E_F) = \left\lceil \frac{N}{\xi B} \right\rceil \xi B - N$$

which is graphed against 1/B in the figure 2-3,

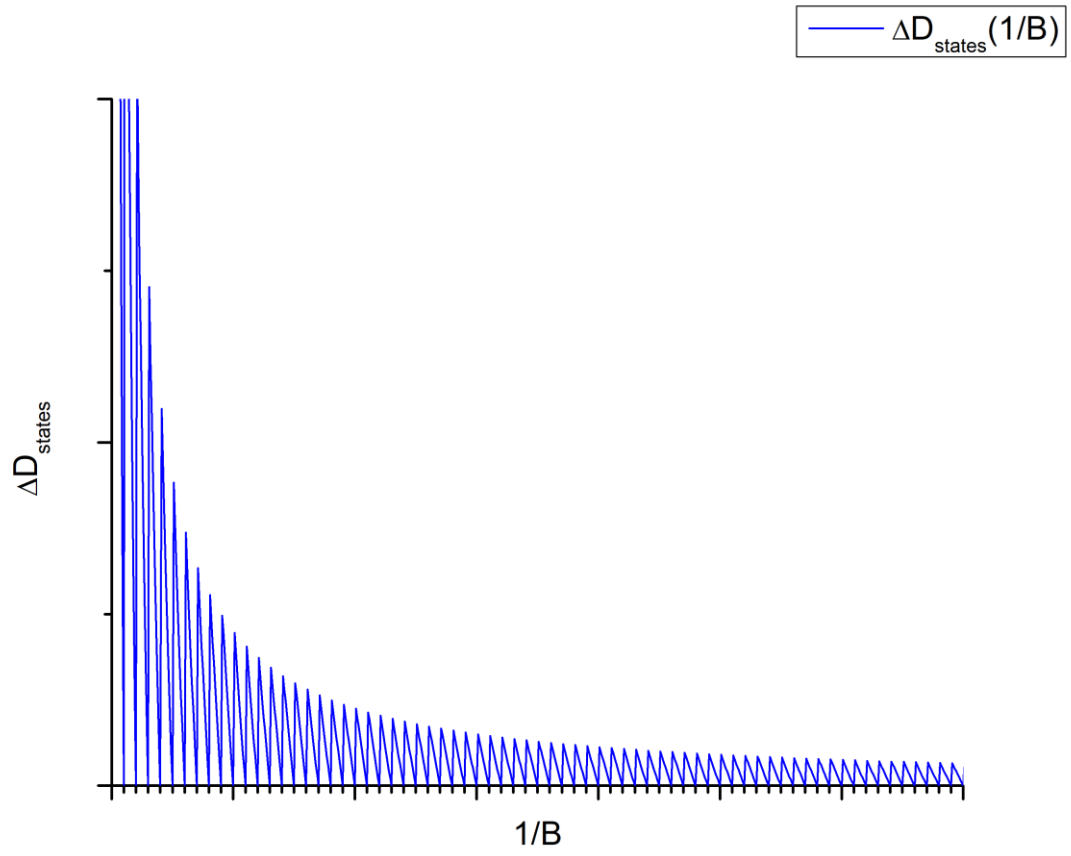


**Figure 2-3** Graph of $\Delta D_{states}$ vs. 1/B. The oscillations can clearly be seen.

which clearly shows there are going to be oscillations in the density of states at the Fermi surface as B is changed.

These quantum oscillations can be described by the Lifshitz Kosevich formula

$$\frac{\Delta\sigma}{\sigma} \propto A_0\sqrt{B}R_T R_D \cos\left[2\pi\left(\frac{F}{B}-\gamma\right)\right]$$

Where $F = \frac{\Phi_0}{2\pi^2}S_k$, which describes the frequency of the oscillations associated with the extremal area $S_k$

The broadening due to time between scattering events is described by $R_D = e^{-\frac{\alpha T_D m^*}{B}}$, the Dingle factor, which has an associated temperature, the Dingle temperature $T_D$, which contains the terms for scattering time. Here, $\alpha = \frac{2\pi^2 k_B}{e\hbar}$ which is a constant. A consequence of the Dingle factor is that heavier effective masses require higher fields to be seen in the oscillations.

The effect of temperature variation on the oscillations is described by $R_T = \frac{\alpha T m^*/B}{\sinh(\alpha T m^*/B)}$. This term covers the smearing of the Landau levels, which become less distinct as temperature is increased. It is through this term that information on the effective mass can be extracted.

The magnetic field modulated microwave spectroscopy (MFMMS) technique measures the reflected microwave power from a sample as a function of temperature [16]. The absorption of this microwave power depends on the surface resistance of the material. When a material undergoes a superconducting transition, for instance, the decrease in resistance causes a reduction in the absorption of microwave power at the surface. Near a superconducting transition, there is a pronounced peak in the MFMMS signal. The MFMMS setup consists of a custom X-band Bruker electron paramagnetic resonance (EPR) apparatus including a microwave power source, a dual-mode cavity resonator, lock-in detector, and a 1 T electromagnet. A sample is placed in the center of a resonant cavity and an automatic frequency controller (AFC) continuously adjusts the frequency of the microwaves to the resonance frequency of the cavity. External dc and ac magnetic fields are also applied in addition to the microwave magnetic field, to enhance the absorption, reduce background noise, and increase the sensitivity. One of the main applications for which the MFMMS technique was developed was to look for superconductors, because of the noninvasive method of testing a sample and the clear signal that they generate.

**Bibliography**


1. P. C. Canfield and Z. Fisk. “Growth of single crystals from metallic fluxes.” *Philosophical Magazine B*, **65** 1117-1123, (1992) DOI: https://doi.org/10.1080/13642819208215073

2. Katsuo Tsukamoto. “24 - In Situ Observation of Crystal Growth and Flows by Optical Techniques.” In Tatau Nishinaga, editor, *Handbook of Crystal Growth (Second Edition)*, pages 1031-1060. Elsevier, Boston, (2015) DOI: http://dx.doi.org/10.1016/B978-0-444-56369-9.00024-1

3. Paweł E. Tomaszewski. “Jan Czochralski-Father of the Czochralski Method.” *Journal of Crystal Growth*, **236** 1-4, (2002) DOI: https://doi.org/10.1016/S0022-0248(01)02195-9

4. Reinhard Uecker. “The Historical Development of the Czochralski Method.” *Journal of Crystal Growth*, **401** 7-24 (2014) DOI: https://doi.org/10.1016/j.jcrysgro.2013.11.095

5. H. Sadamura, H. Fujii, and T. Okamoto. “Czochralski Crystal Growth of Intermetallics Compounds by Use of a Tri-Arc Furnace.” *IEEE Translation Journal on Magnetics in Japan*, **1** 810-811, (1985) DOI: https://doi.org/10.1109/TJMJ.1985.4548970

6. Michael P. Marder. “Condensed Matter Physics” **2** John Wiley & Sons Inc. (2010) ISBN 978-0-470-61798-4

7. Elliot Snider, Nathan Dasenbrock-Gammon, Raymond McBride, Xiaoyu Wang, Noah Meyers, Keith V. Lawler, Eva Zurek, Ashkan Salamat, and Ranga P. Dias. “Synthesis of Yttrium Superhydride Superconductor with a Transition Temperature up to 262 K by Catalytic Hydrogenation at High Pressures.” *Phys. Rev. Lett.*, **126** 117003, (2021) DOI: https://doi.org/10.1103/PhysRevLett.126.117003

8. P. Bredy, J. Belorgey, P. Chesny, B. Hervieu, H. Lannou, F. P. Juster, W. Abdel-Maksoud, C. Mayri, F. Molinie, and A. Payn. “Cryogenics Around the 11.7 T MRI Iseult Magnet.” *IEEE Transactions on Applied Superconductivity*, **20** 2066-2069, (2010) DOI: https://doi.org/10.1109/TASC.2010.2040160

9. J. P. Torre and G. Chanin. “Miniature Liquid-$^3$He Refrigerator.” *Review of Scientific Instruments*, **56** 318-320, (1985) DOI: https://doi.org/10.1063/1.1138350

10. A. T. A. M. De Waele. “Basic Operation of Cryocoolers and Related Thermal Machines.” *Journal of Low Temperature Physics*, **164** 179-236, (2011) DOI: https://doi.org/10.1007%2Fs10909-011-0373-x

11. Quantum Design, Inc. (2011) [Online]. Available: http://www.qdusa.com/products/dynacool.html

12. J. File and R. G. Mills. “Observation of Persistent Current in a Superconducting Solenoid.” *Phys. Rev. Lett.*, **10** 93-96, (1963) DOI: https://doi.org/10.1103/PhysRevLett.10.93

13. Marcelo Jaime, Carolina Corvalán Moya, Franziska Weickert, Vivien Zapf, Fedor F. Balakirev, Mark Wartenbe, Priscila F. S. Rosa, Jonathan B. Betts, George Rodriguez, Scott A. Crooker, and Ramzy Daou. “Fiber Bragg Grating Dilatometry in Extreme Magnetic Field and Cryogenic Conditions.” *Sensors*, **17**, (2017) DOI: https://doi.org/10.3390/s17112572

14. M. M. Altarawneh, C. H. Mielke, and J. S. Brooks. “Proximity Detector Circuits: An Alternative to Tunnel Diode Oscillators for Contactless Measurements in Pulsed Magnetic Field Environments.” *Review of Scientific Instruments*, **80** 066104, (2009) DOI: https://doi.org/10.1063/1.3152219

15. Charles Kittel. “Introduction to Solid State Physics” **8** John Wiley & Sons, Inc (2005) ISBN 978-0-471-41526-8

16. Juan Gabriel Ramírez, Ali C. Basaran, J. de la Venta, Juan Pereiro, and Ivan K. Schuller. “Magnetic Field Modulated Microwave Spectroscopy Across Phase Transitions and the Search for New Superconductors.” *Reports on Progress in Physics*, **77** 093902, (2014). DOI: http://dx.doi.org/10.1088/0034-4885/77/9/093902

## Chapter 3: Quantum Oscillations in $PrT_2Cd_{20}$ ($T$ = Ni, Pd)

### Introduction

A family of "cage" compounds of the form $RM_2X_{20}$, where $R$ is a rare earth element, $M$ is a transition metal, and $X$ and an $s$-$p$ metal such as Al, Zn, or Cd, have attracted much interest because they exhibit various correlated electron phenomena such as Kondo lattice behavior, valence fluctuations, heavy fermion behavior, unconventional types of superconductivity, and exotic types of magnetic and quadrupolar order [1, 2, 3, 4]. The $RM_2X_{20}$ "1-2-20" compounds crystallize in the cubic $CeCr_2Al_{20}$-type structure, which is comprised of two types of atomic cages, one containing the $R$ ion and the other containing the $M$ ion. The hybridization of the localized $f$- and $d$-electron states of the $R$ or $M$ "guest" ions with the ligand states of the surrounding ions of the atomic cages can generate strong electronic correlations. Since these "cage" compounds contain both $R$ and $M$ ions, it seems possible that the $R$ and $M$ ions could act in concert and produce new types of emergent quantum phenomena.

The Pr-based "1-2-20" compounds have special physical properties that can be traced to (1) the hybridization of the localized $Pr^{3+}$ 4$f$ electron states and the ligand states of the 16 surrounding $X$ "cage" ions and (2) the ground state of $Pr^{3+}$ in the cubic crystalline electric field (CEF). In a cubic CEF, the J = 4 multiplet of the $Pr^{3+}$ ion splits into four states: a $\Gamma_1$ singlet, a $\Gamma_3$ non-Kramers doublet, and $\Gamma_4$ and $\Gamma_5$ triplets [5]. The $\Gamma_3$ doublet appears to be the ground state in many of the $PrM_2X_{20}$ compounds [3, 6, 7]. The nonmagnetic quadrupolar degrees of freedom of the $\Gamma_3$ ground state and the localized $f$-electron-ligand state hybridization are the basic ingredients for a quadrupolar Kondo effect (QKE), a variant of a 2-channel spin-1/2 Kondo effect [8, 9], and exotic types of quadrupolar order. Recently, evidence for a QKE has been

found in several $PrT_2X_{20}$ compounds with a nonmagnetic non-Kramers $\Gamma_3$ ground state in the cubic CEF. The compounds $PrTi_2Al_{20}$ [7] and $PrV_2Al_{20}$ [10] have been reported to display unconventional superconductivity with $T_c$'s of 0.2 K and 0.06 K, respectively. The superconductivity coexists with ferroquadrupolar (FQ) order in $PrTi_2Al_{20}$ ($T_{FQ}$ = 2 K) and antiferroquadrupolar (AFQ) order in $PrV_2Al_{20}$ ($T_{AFQ}$ = 0.6 K). The compounds PrRh2Zn20 and PrIr2Zn20 have also been reported to exhibit AFQ order [3].

A QKE was first suggested to account for several of the striking properties of the superconducting heavy fermion compound $UBe_{13}$ [8]. Subsequently, an unconventional Kondo effect with non-Fermi liquid (NFL) characteristic at low temperatures was discovered in the pseudoternary system $Y_{1-x}U_xPd_3$ [11, 12]. Many of the properties of the $Y_{1-x}U_xPd_3$ system were shown to be consistent with the presence of a $U^{4+}$ $\Gamma_3$ ground state in the cubic CEF and the predictions of the QKE [11, 13, 14, 15]. The low-$T$ NFL characteristics scale with the Kondo temperature $T_K$ and the U concentration and have the following $T$-dependences: The electrical resistivity $\rho(T)$ varies as -$T$, the specific heat divided by temperature $C(T)/T$ diverges as -log($T$) with evidence of a residual entropy S(0) = (1/2)Rlog(2), and the magnetic susceptibility $\chi(T)$ varies as $T^{1/2}$. Except for $\rho(T)$, these properties were found to be consistent with theoretical predictions based on the single ion QKE. It was later predicted theoretically that $\rho(T)$ varies as $T^{1/2}$ for the single ion QKE. Interestingly, the linear $T$-dependence of $\rho(T)$ and the -log($T$) divergence of $C(T)/T$ observed in the $Y_{1-x}U_xPd_3$ system have become hallmarks of NFL behavior in many quantum critical *f*-electron systems [13, 14, 16, 17]. It was conjectured that the linear $T$-dependence of $\rho(T)$ in the $Y_{1-x}U_xPd_3$ system could be due to interactions between U ions at the U concentrations investigated. The Pr-based "1-2-20" $PrT_2X_{20}$ "cage" compounds with a non-Kramers $\Gamma_3$ ground state in the cubic CEF offer new opportunities to study QKE

phenomena. In comparison with cubic U-based compounds, cubic Pr-based compounds are more favorable for studies of the QKE because of the greater stability of the $f^2$ configuration but less favorable as a result of smaller *f*-electron – conduction electron hybridization.

In a recent theoretical study, van Dyke, Zhang and Flint [18] found that cubic Pr-based compounds with a $\Gamma_3$ non-Kramers doublet ground state can exhibit a novel heavy Fermi liquid state with spinorial hybridization ("hastatic" order) that breaks time reversal symmetry. They noted that a heavy Fermi liquid stabilized in intermediate magnetic fields has been found in several Pr-based "1-2-20" materials. A simple realistic microscopic model of ferrohastatic order developed by the authors yielded predictions of physical properties and behavior in a magnetic field that may account for the observation of heavy Fermi liquids at intermediate fields in the $Pr(Ir, Rh)_2Zn_{20}$ system. They constructed the Landau theory of ferrohastatic order, allowing a description of its behavior close to the transition and its thermodynamic characteristics from magnetic susceptibility to thermal expansion.

In 2014, our group discovered a family of $RM_2X_{20}$ compounds with $X$ = Cd [19]. Exploratory experiments were carried out on many of these compounds for several $R$ ions with unstable valence, Ce, Pr, and Sm, and the transition metal ions $M$ = Ni, Pd, to search for emergent correlated electron behavior. Initial studies yielded evidence for the following general types of behavior: $CeM_2Cd_{20}$ ($M$ = Ni, Pd) – weak hybridization and isolated localized Ce magnetic moments [20], $PrM_2Cd_{20}$ ($M$ = Ni, Pd) – nonmagnetic $\Gamma_1$ or $\Gamma_3$ ground state for $Pr^{3+}$ [21], and $SmM_2Cd_{20}$ ($M$ = Ni, Pd) – heavy Fermi liquid and FM and AFM order.

The studies of $PrNi_2Cd_{20}$ and $PrPd_2Cd_{20}$ explored their physical properties and attempted to discover their ground states the ground state of $Pr^{3+}$ in the cubic CEF. The electrical

resistivity, specific, heat, and magnetization all indicate the presence of strong electronic correlations in these compounds, suggesting the effective mass could be large, with the correlations appearing to be stronger in $PrPd_2Cd_{20}$ [21]. As noted above, the ground state has been identified as the $\Gamma_3$ doublet in many of the Pr-based 1-2-20 compounds [21]. This is an interesting scenario, since the $\Gamma_3$ doublet can give rise to a quadrupolar Kondo effect with non-Fermi liquid behavior at low temperatures, as appears to have been realized in $PrV_2Al_{20}$ and $PrTi_2Al_{20}$ [7, 22]. Ultrasonic and specific heat measurements indicate that the $\Gamma_3$ doublet is indeed the ground state in $PrNi_2Cd_{20}$ and $PrPd_2Cd_{20}$ [23, 24]. Specific heat measurements were also used to examine the strengths of the interactions between the two-level systems in these compounds and found that the interactions in $PrNi_2Cd_{20}$ were weak enough to be neglected, but the interactions in $PrPd_2Cd_{20}$ were strong enough to promote magnetic or multipolar ordering at low temperatures [24].

Quantum oscillations are a way to measure the Fermi surface of a material. In the presence of a magnetic field, electron orbitals reorganize themselves. As these electron orbitals cross the Fermi surface, there are fluctuations in the density of states that can indicate the spatial extent of the Fermi surface. These fluctuations in the density of states can be seen in observable quantities such as electrical conductivity and magnetic susceptibility. Importantly, quantum oscillations can also help to identify the effective masses of quasiparticles within the system. This allows the use of quantum oscillation measurements to investigate the large effective masses suggested by the specific heat, electrical resistivty and magnetization measurements [21]. Because these effective masses are potentially high, they can be more clearly detected in quantum oscillations measurements in high magnetic fields and at low temperatures, so the quantum oscillation measurements were made in pulsed high magnetic fields up to 60 tesla.

Quantum oscillations measurements can also be used to suggest the presence of a topological state [25].

**Experimental Procedure**

Single crystals of $PrNi_2Cd_{20}$ and $PrPd_2Cd_{20}$ were grown using a flux growth method. The elements were mixed in a 1-2-48 ratio to use Cd as a flux in an alumina crucible [19]. This was sealed inside a quartz tube and heated to 700 °C for 6 hours before being cooled at 2 °C per hour to 500 °C at which point the samples were centrifuged to remove excess flux. This resulted in large single crystals which were then oriented using a Laue X ray machine, using freely available crystal orientation software Clip [26]. Samples were measured at Los Alamos National Laboratory National High Magnetic Field Laboratory (NHML) using a Proximity Detector Oscillator (PDO) method for measuring the oscillations in the resistivity while in a pulsed magnetic field, in fields up to 60 tesla [27, 28]. PDO measurements use an RF sensor coil to allow measuring oscillations through the changes in the skin-depth of the material [28]. Samples were rotated about the [1-11], [001], and [-110] directions on a sample rotator and cooled down to ~1.5K by pumping on $He^4$. Temperature dependent measurements were conducted with the field parallel to the [111] direction from 30 K down to 0.5 K, with the lowest temperatures reached by pumping on $He^3$.

A Fermi-surface model of $LaNi_2Cd_{20}$ was produced by Full potential Augmented Plane Wave Method (FLAPW) with Local Density Approximation (LDA) for the exchange potential using KANSAI code [29]. From this model expected SdH curves were derived. $LaNi_2Cd_{20}$ was used because the expected contribution from localized *f*-electrons from the Pr was not expected to contribute much to the band structure, and is also difficult to model.

**Results and Discussion**

Typical results showing the quantum oscillations can be seen in Figure 3-1. Figure 3-2 shows a typical Fourier transform of the same data. Fourier transforms were taken with various windows to check for the consistency of the oscillation frequencies in the complex spectra. Those peaks that could be potentially the harmonics of earlier peaks were identified, with a visual judgment of how close the identified value was to a possible harmonic frequency. Obvious second harmonics were removed.

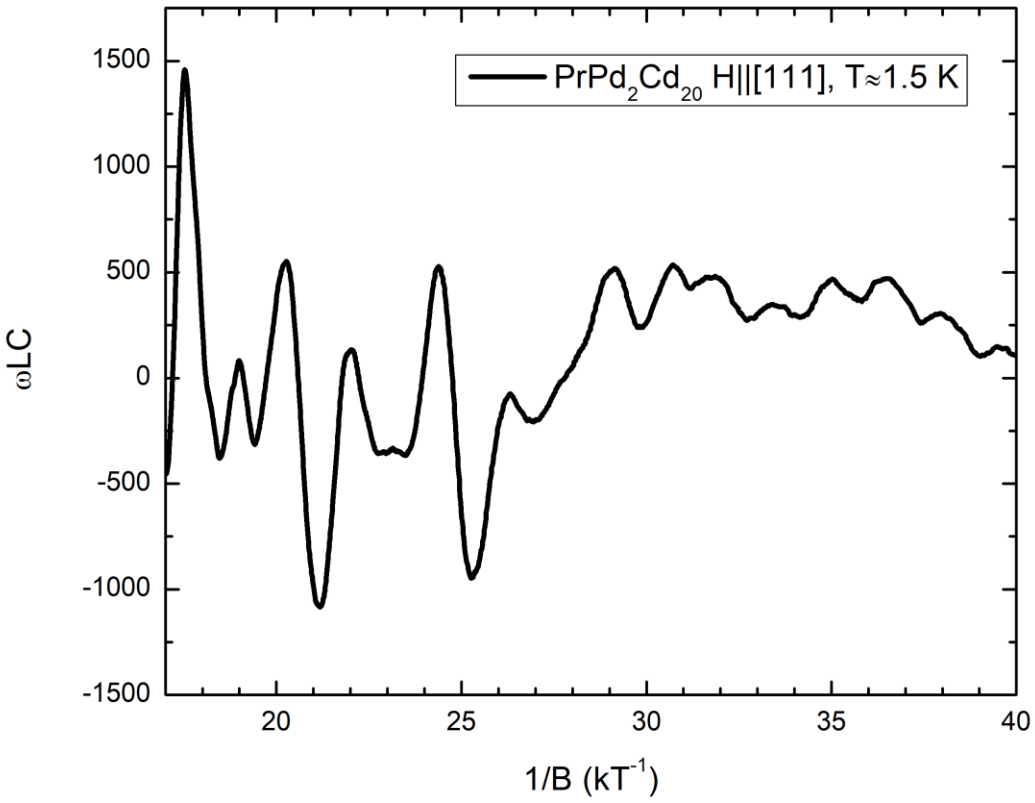


**Figure 3-1** Quantum oscillations of $PrPd_2Cd_{20}$ with the magnetic field parallel to the [111] direction as an example of the typical quantum oscillation results in these systems.

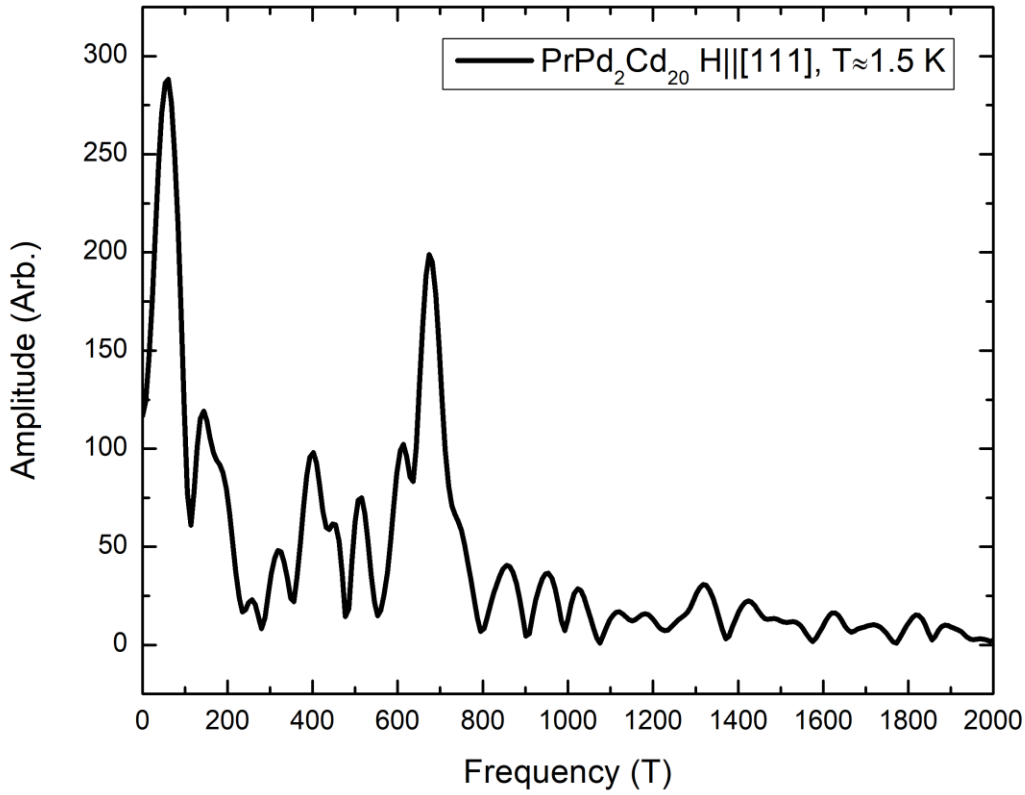


**Figure 3-2** Fourier transform of quantum oscillations of $PrPd_2Cd_{20}$ with the magnetic field parallel to the [111] direction as an example of the typical results in these systems.

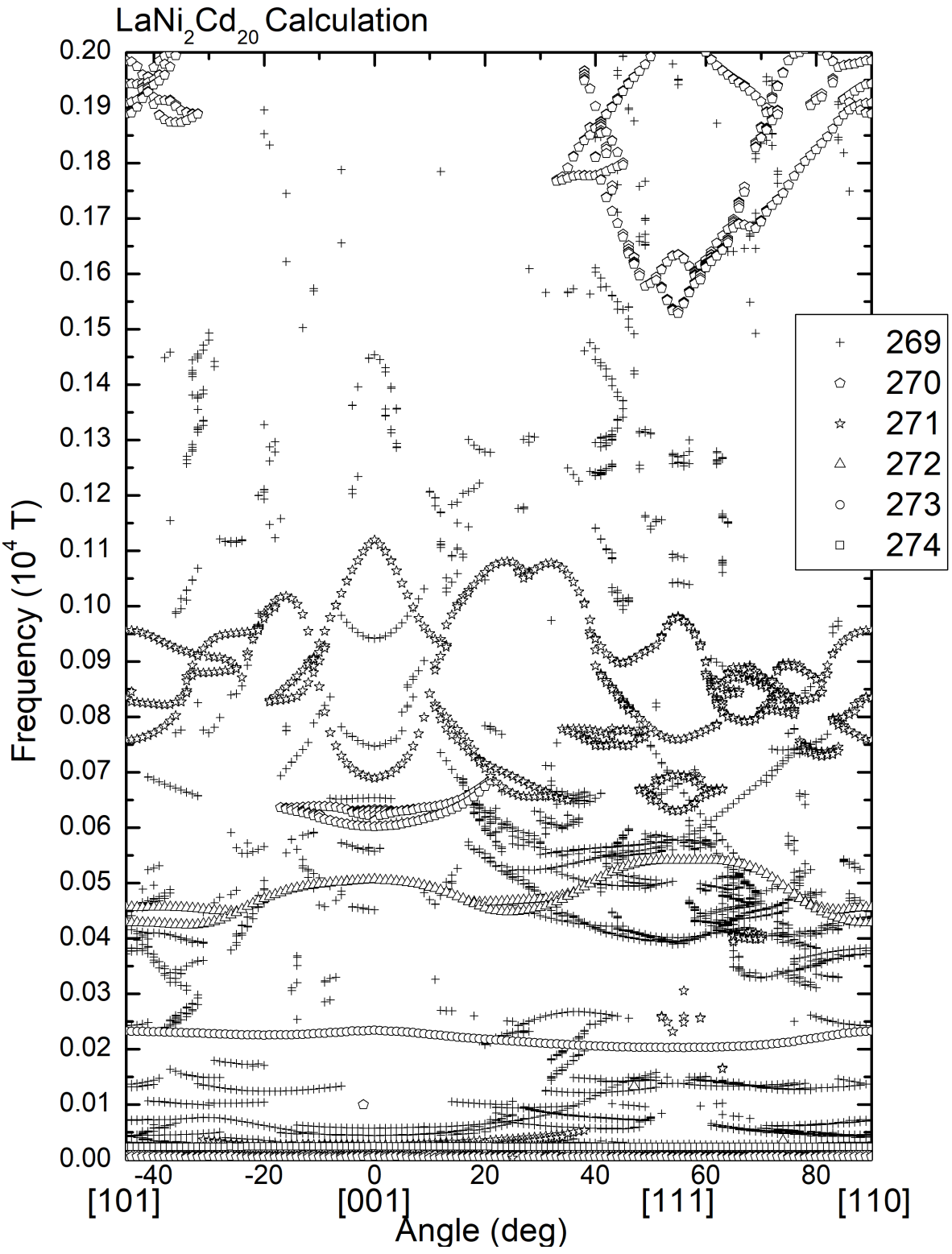


**Figure 3-3** Results of FLAPW calculations of $LaNi_2Cd_{20}$. The numbers (269-274) in the legend refer to the Fermi surface contributions from the 269$^{th}$ through 274$^{th}$ electron bands.

The peaks in the Fourier transforms were tracked across the measurements as a function of angle. The resulting graph can be compared to the results of the FLAPW calculations of $LaNi_2Cd_{20}$ as in Figure3-3. These comparisons are made in Figures 3-4 and 3-5 for $PrNi_2Cd_{20}$ and $PrPd_2Cd_{20}$ respectively. We can see good agreement in various sections, as well as some disagreements especially when comparing $PrPd_2Cd_{20}$. These agreements are expected since they are both 1-2-20 systems, but as they are different systems they are not expected to be perfectly similar, and as can be expected by the lattice parameters (15.699 Å for $PrPd_2Cd_{20}$, 15.575 Å for $PrNi_2Cd_{20}$, and 15.584 Å for $LaNi_2Cd_{20}$ [19] )the $PrPd_2Cd_{20}$ is less similar than the $PrNi_2Cd_{20}$. Differences are expected to be due to the impact of the localized *f*-electrons from the Pr on the system.

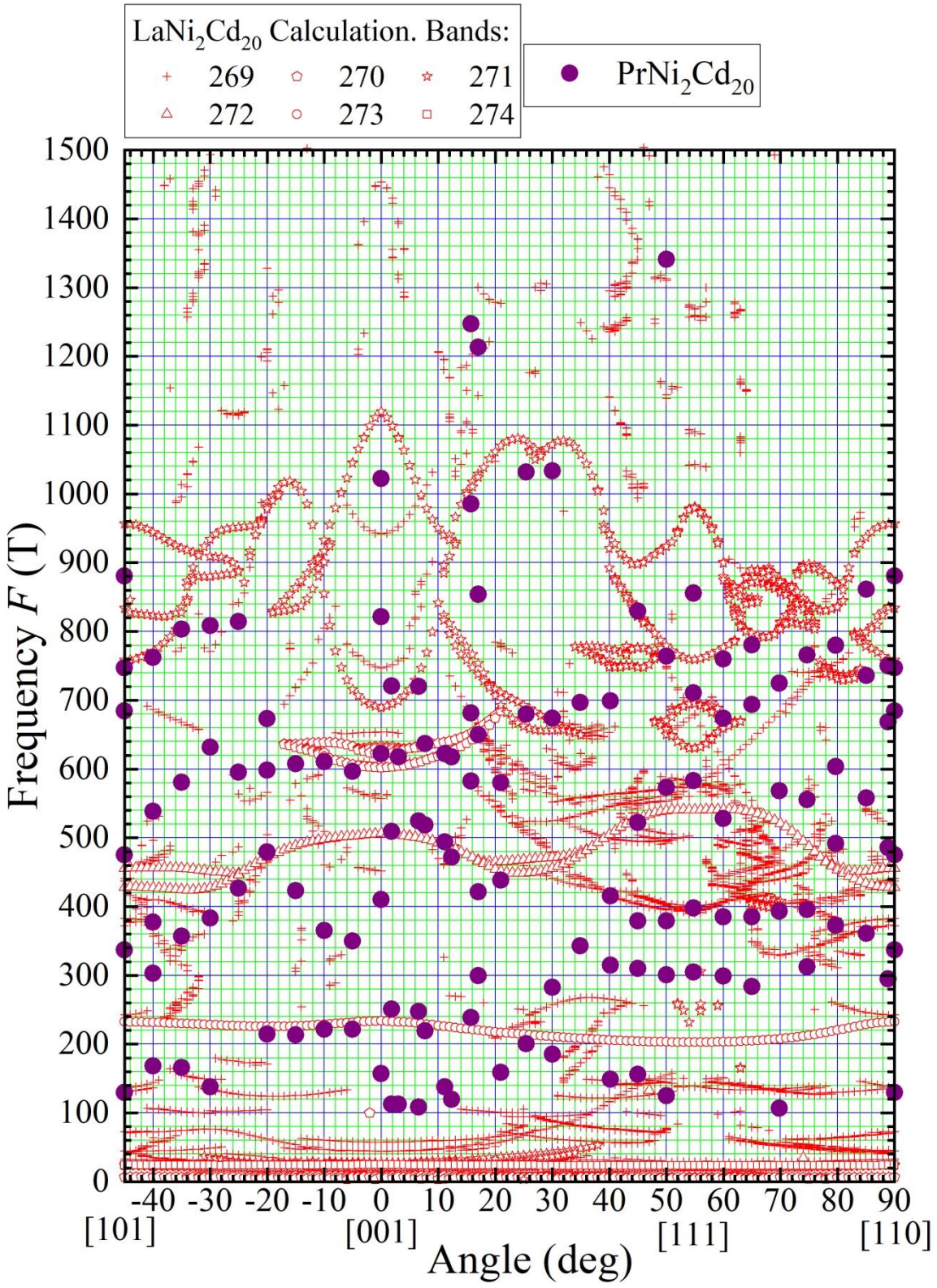


**Figure 3-4** The purple points indicate peaks in the experimental data for $PrNi_2Cd_{20}$. The red points are included for comparison and indicate the theoretical $LaNi_2Cd_{20}$ data

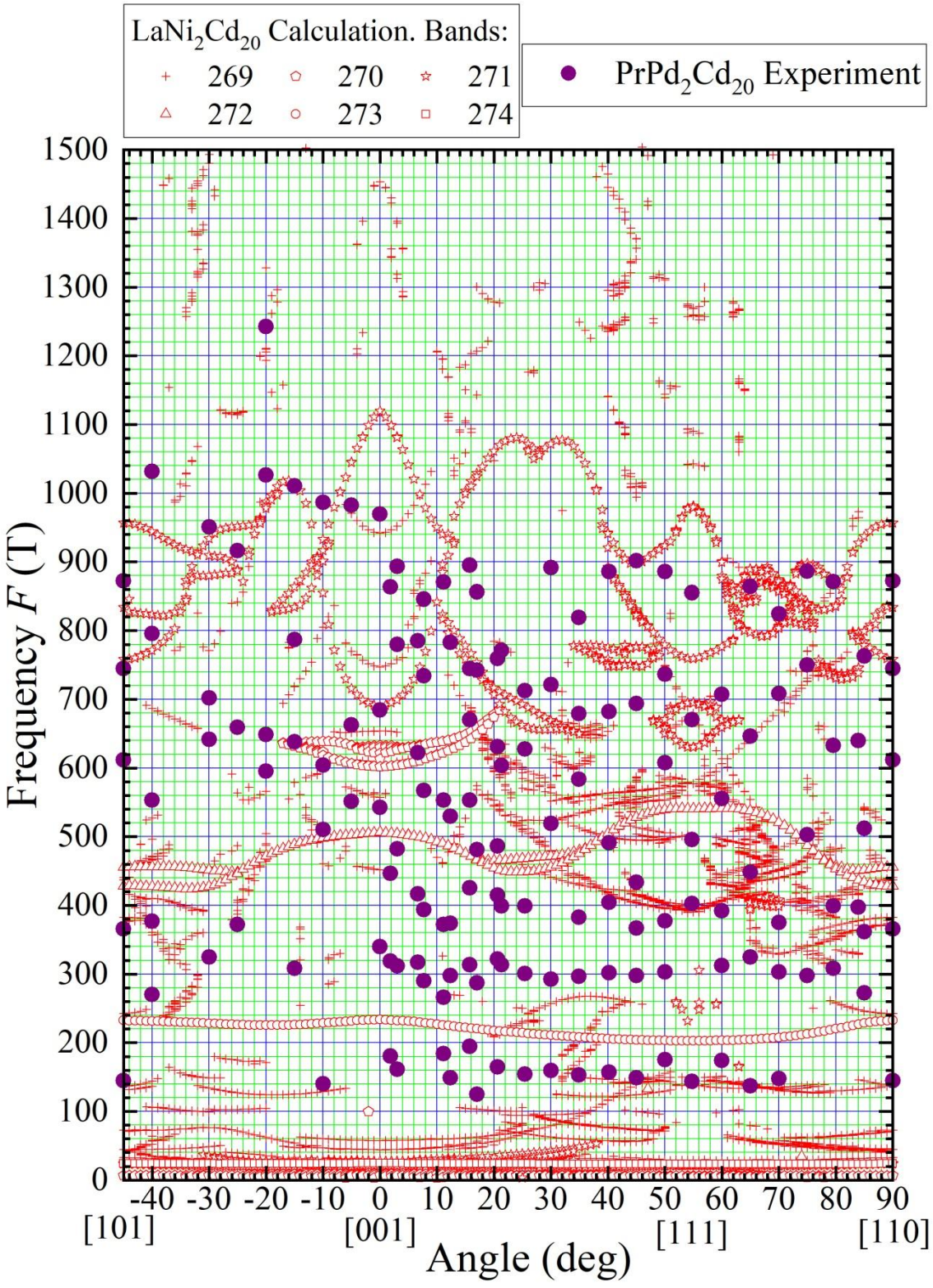


**Figure 3-5** The purple points indicate peaks in the experimental data for $PrPd_2Cd_{20}$. The red points are included for comparison and indicate the theoretical $LaNi_2Cd_{20}$ data

One notable difference is that the SdH oscillations which seem to correspond to $LaNi_2Cd_{20}$'s 273$^{rd}$ electron band, which do not exhibit a strong angular dependence and thus indicate a roughly spherical Fermi surface associated with this band, appears to be at a higher frequency in $PrPd_2Cd_{20}$ compared to $PrNi_2Cd_{20}$ and $LaNi_2Cd_{20}$.

A large part of the complexity of the Fermi surfaces of these compounds is associated with the 269 band electrons, as apparent in the theoretical graphs of the Fermi surfaces in Figure 3-6. The complexity of the oscillation spectra and the Fermi surface in general is comparable to that of other Pr 1-2-20 systems such as $PrTi_2Al_{20}$ [30].

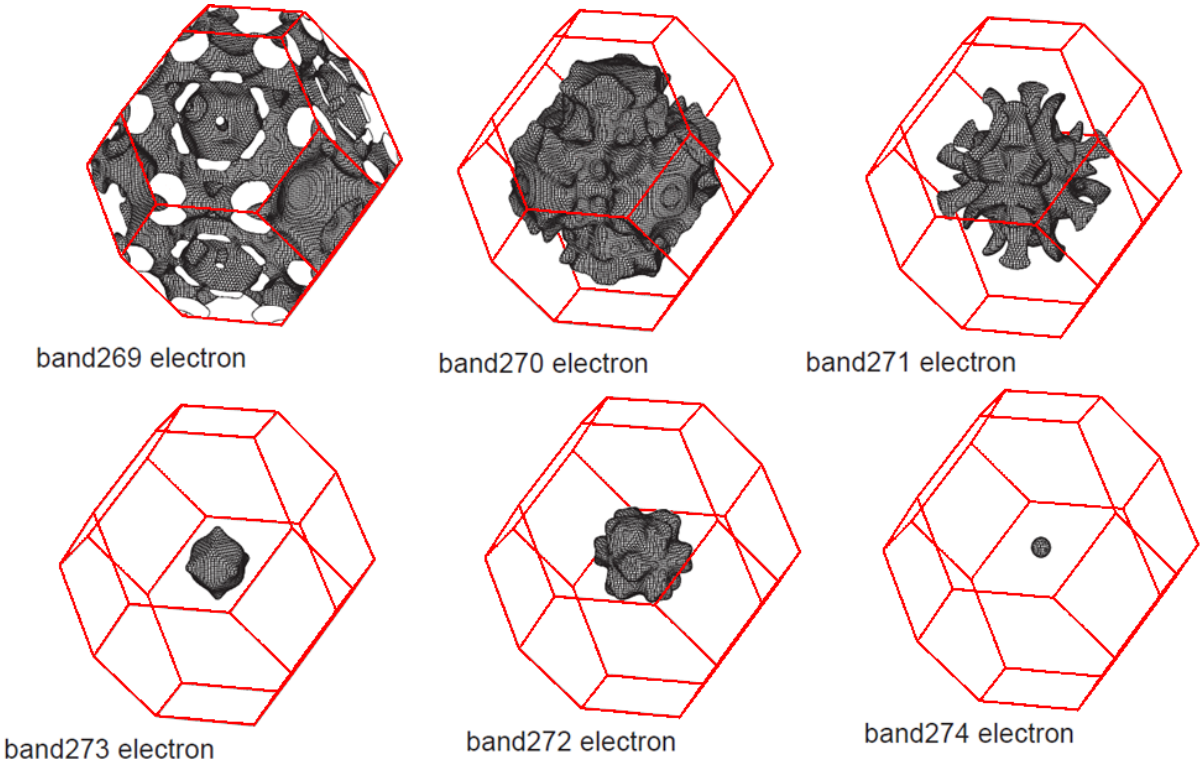


**Figure 3-6** Theoretical Fermi surfaces generated by the FLAPW calculations for $LaNi_2Cd_{20}$

The Lifshitz Kosevich relation $\frac{R_T}{T} = A_0 \frac{\alpha m^*/H}{\sinh(\alpha m^*/H)}$ can be used to compute the effective mass of samples associated with different Fermi surfaces of the compound [31]. A fitting to this formula can be seen in figure 3-7. A graph comparing the theoretical masses to our experimental masses can be seen in figure 3-8. The agreement is fairly good, with some heavier masses being indicated at around 710 T in the case of $PrNi_2Cd_{20}$ and around 400 T in the case of $PrPd_2Cd_{20}$. This is in contrast to the resistivity, specific heat, and magnetization data which suggested strong correlations [21]. It is possible that this data is not seen because the effective masses are too high and require higher fields or lower temperatures to be observed in a quantum oscillation measurement.

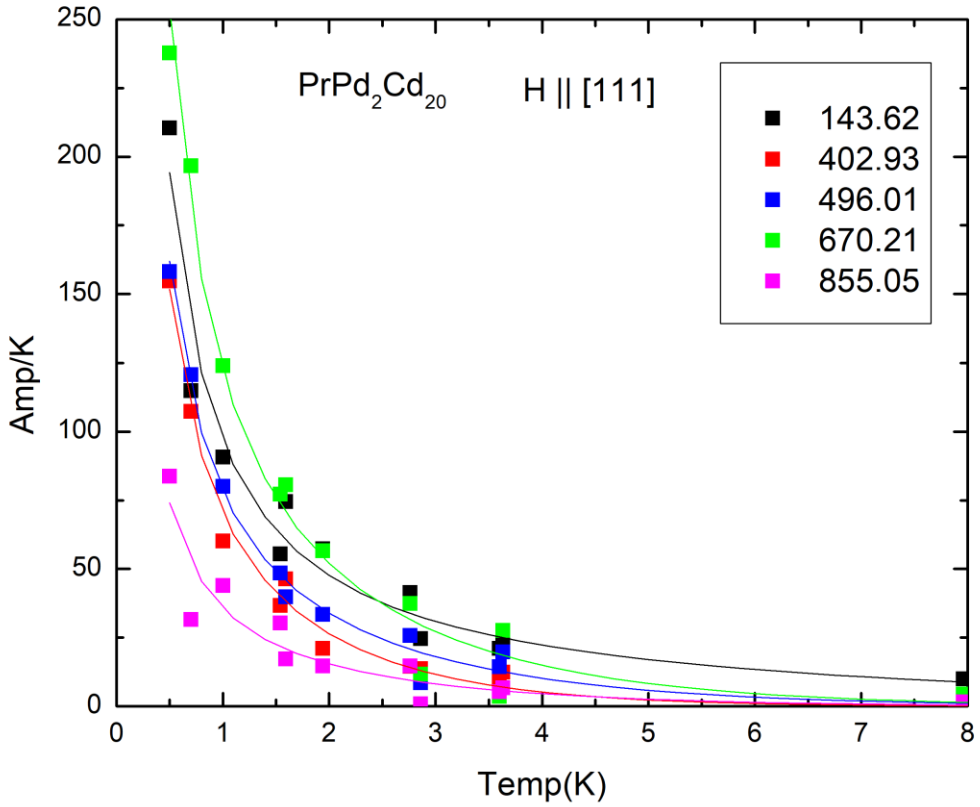


**Figure 3-7** Amplitude divided by temperature data versus temperature for the peaks around 105.9 tesla. The line is the fit to the Lifshitz Kosevich formula.

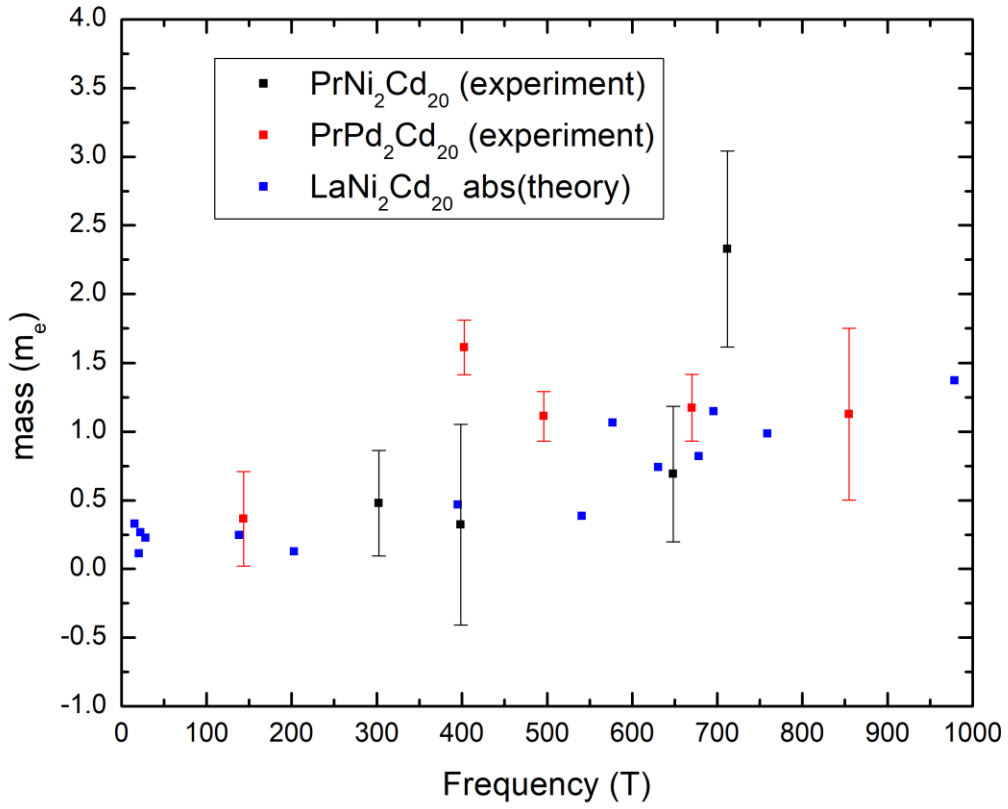


**Figure 3-8** Comparison of the experimentally determined mass values as a function of frequency with the absolute value of those of predicted by theoretical calculations.

**Acknowledgements**

The National High Magnetic Field Laboratory is supported by the National Science Foundation through NSF/DMR-1157490/1644779 and the State of Florida. Research at UCSD was supported by the US DOE BES under Grant No. DE-FG02-04-ER46105 (materials synthesis and characterization), the US NSF under Grant No. DMR-1206553 (low temperature measurements), and the NNSA under the SSAA program through the US DOE under Grant No. DE-NA0002909 (high field measurements) This research is also funded by a QuantEmX grant

from ICAM and the Gordon and Betty Moore Foundation through Grant GBMF5305 to Alexander Breindel

Chapter 3, in full, is currently being prepared for submission for publication of the material. Ran, Sheng; Balakirev, Fedor; Singleton, John; Harima, Hisatomo; Maple, M. Brian. The dissertation author was the primary investigator and author of this material.

## Bibliography


1. M. S. Torikachvili, S. Jia, E. D. Mun, S. T. Hannahs, R. C. Black, W. K. Neils, Dinesh Martien, S. L. Bud'ko, and P. C. Canfield. "Six closely related $YbT_2Zn_{20}$ (T = Fe, Co, Ru, Rh, Os, Ir) heavy fermion compounds with large local moment degeneracy," *Proceedings of the National Academy of Sciences* **104,** 9960-9963 (2007), DOI: https://doi.org/10.1073/pnas.0702757104

2. E. D. Bauer, C. Wang, V. R. Fanelli, J. M. Lawrence, E. A. Goremychkin, N. R. de Souza, F. Ronning, J. D. Thompson, A. V. Silhanek, V. Vildosola, A. M. Lobos, A. A. Aligia, S. Bobev, and J. L. Sarrao. "Simplifying strong electronic correlations in uranium: Localized uranium heavy-fermion $UM_2Zn_{20}$ (M = Co, Rh) compounds," *Phys. Rev. B* **78,** 115120 (2008), DOI: https://doi.org/10.1103/PhysRevB.78.115120

3. Takahiro Onimaru and Hiroaki Kusunose. "Exotic quadrupolar phenomenain non-kramers doublet systems - the cases of $PrT_2Zn_{20}$ (T = Ir, Rh) and $PrT_2Al_{20}$ (T = V, Ti) - ," *Journal of the Physical Society of Japan* **85,** 082002 (2016), DOI: https://doi.org/10.7566/JPSJ.85.082002

4. Yoshiya Uwatoko, Hiroki Takahashi, and Gendo Oomi. "Chapter 295 - effect of pressure on the interplay between orbital and magnetic ordering, kondo effect, valence fluctuations, and superconductivity in rare-earth compounds." In Jean-Claude G. Bünzli and Vitalij K. Pecharsky, editors, *Including Actinides, volume 51 of Handbook on the Physics and Chemistry of Rare Earths*, pages 1-109. Elsevier (2017), DOI: https://doi.org/10.1016/bs.hpcre.2017.01.001

5. K. R. Lea, M. J. M. Leask, and W. P. Wolf. "The raising of angular momentum degeneracy of *f*-electron terms by cubic crystal fields," *Journal of Physics and Chemistry of Solids* **23,** 1381-1405 (1962), DOI: https://doi.org/10.1016/0022-3697(62)90192-0

6. Akito Sakai and Satoru Nakatsuji. "Kondo effects and multipolar order in the cubic $PrTr_2Al_{20}$ (Tr = Ti, V)," *Journal of the Physical Society of Japan* **80**, 063701 (2011), DOI: https://doi.org/10.1143/JPSJ.80.063701

7. Akito Sakai, Kentaro Kuga, and Satoru Nakatsuji. "Superconductivity in the ferroquadrupolar state in the quadrupolar Kondo lattice $PrTi_2Al_{20}$," *Journal of the Physical Society of Japan* **81**, 083702 (2012), DOI: https://doi.org/10.1143/JPSJ.81.083702

8. D. L. Cox. "Quadrupolar kondo effect in uranium heavy-electron materials?" *Phys. Rev. Lett.* **59**, 1240-1243 (1987), DOI: https://doi.org/10.1103/PhysRevLett.59.1240

9. D. L. Cox and M. Jarrell. "The two-channel kondo route to non-fermi-liquid metals," *Journal of Physics: Condensed Matter* **8**, 9825-9853 (1996), DOI: https://doi.org/10.1088/0953-8984/8/48/012

10. Yosuke Matsumoto, Masaki Tsujimoto, Takahiro Tomita, Akito Sakai, and Satoru Nakatsuji. “Heavy fermion superconductivity in non-magnetic cage compound $PrV_2Al_{20}$,” *Journal of Physics: Conference Series* **683,** 012013 (2016), DOI: https://doi.org/10.1088/1742-6596/683/1/012013

11. C. L. Seaman, M. B. Maple, B. W. Lee, S. Ghamaty, M. S. Torikachvili, J.-S. Kang, L. Z. Liu, J. W. Allen, and D. L. Cox. “Evidence for non-fermi liquid behavior in the kondo alloy $Y_{1-x}U_xPd_3$,” *Phys. Rev. Lett.* **67,** 2882-2885 (1991), DOI: https://doi.org/10.1103/PhysRevLett.67.2882

12. B. Andraka and A. M. Tsvelik. “Observation of non-fermi-liquid behavior in $U_{0.2}Y_{0.8}Pd_3$,” *Phys. Rev. Lett.* **67,** 2886-2889 (1991), DOI: https://doi.org/10.1103/PhysRevLett.67.2886

13. M. B. Maple, C. L. Seaman, D. A. Gajewski, Y. Dalichaouch, V. B. Barbetta, M. C. de Andrade, H. A. Mook, H. G. Lukefahr, O. O. Bernal, and D. E. MacLaughlin. “Non fermi liquid behavior in strongly correlated *f*-electron materials,” *Journal of Low Temperature Physics* **95,** 225-243 (1994), DOI: https://doi.org/10.1007/BF00754938

14. M. B. Maple, M. C. de Andrade, J. Herrmann, Y. Dalichaouch, D. A. Gajewski, C. L. Seaman, R. Chau, R. Movshovich, M. C. Aronson, and R. Osborn. “Non fermi liquid ground states in strongly correlated *f*-electron materials,” *Journal of Low Temperature Physics* **99**, 223-249 (1995), DOI: https://doi.org/10.1007/BF00752290

15. M. Brian Maple, Ryan E. Baumbach, Nicholas P. Butch, James J. Hamlin, and Marc Janoschek. “Non-fermi liquid regimes and superconductivity in the low temperature phase diagrams of strongly correlated *d*- and *f*-electron materials,” *Journal of Low Temperature Physics* **161,** 4-54 (2010), DOI: https://doi.org/10.1007/s10909-010-0212-5

16. G. R. Stewart. “Non-fermi-liquid behavior in *d*- and *f*-electron metals,” *Rev. Mod. Phys.* **73,** 797-855 (2001), DOI: https://doi.org/10.1103/RevModPhys.73.797

17. Hilbert v. Löhneysen, Achim Rosch, Matthias Vojta, and Peter Wölfle. “Fermi-liquid instabilities at magnetic quantum phase transitions,” *Rev. Mod. Phys.* **79**, 1015-1075 (2007), DOI: https://doi.org/10.1103/RevModPhys.79.1015

18. John S. Van Dyke, Guanghua Zhang, and Rebecca Flint. “Field-induced ferrohastatic phase in cubic non-kramers doublet systems,” *Phys. Rev. B* **100**, 205122 (2019), DOI: https://doi.org/10.1103/PhysRevB.100.205122

19. V.W. Burnett, D. Yazici, B. D. White, N. R. Dilley, A. J. Friedman, B. Brandom, and M. B. Maple. “Structure and physical properties of $RT_2Cd_{20}$ (R = rare earth, T = Ni, Pd) compounds with the $CeCr_2Al_{20}$-type structure,” *Journal of Solid State Chemistry* **215**, 114-121 (2014), DOI: https://doi.org/10.1016/j.jssc.2014.03.035

20. B. D. White, D. Yazici, P-C Ho, N. Kanchanavatee, N. Pouse, Y. Fang, A. J. Breindel, A. J. Friedman, and M. B. Maple. "Weak hybridization and isolated localized magnetic moments in the compounds $CeT_2Cd_{20}$ (T = Ni, Pd)," *Journal of Physics: Condensed Matter* **27**, 315602 (2015), DOI: https://doi.org/10.1088/0953-8984/27/31/315602

21. D. Yazici, T. Yanagisawa, B. D. White, and M. B. Maple. "Nonmagnetic ground state in the cubic compounds $PrNi_2Cd_{20}$ and $PrPd_2Cd_{20}$," *Phys. Rev. B* **91**, 115136 (2015), DOI: https://doi.org/10.1103/PhysRevB.91.115136

22. Masaki Tsujimoto, Yosuke Matsumoto, Takahiro Tomita, Akito Sakai, and Satoru Nakatsuji. "Heavy-fermion superconductivity in the quadrupole ordered state of $PrV_2Al_{20}$," *Phys. Rev. Lett.* **113**, 267001 (2014), DOI: https://doi.org/10.1103/PhysRevLett.113.267001

23. Tatsuya Yanagisawa, Hiroyuki Hidaka, Hiroshi Amitsuka, Shintaro Nakamura, Satoshi Awaji, Elizabeth L. Green, Sergei Zherlitsyn, Joachim Wosnitza, Duygu Yazici, Benjamin. D. White, and M. Brian Maple. "Quadrupolar susceptibility and magnetic phase diagram of $PrNi_2Cd_{20}$ with non-Kramers doublet ground state," *Philosophical Magazine* **100**, 1268-1281 (2019), DOI: https://doi.org/10.1080/14786435.2019.1709912

24. A. M. Konic, R. B. Adhikari, A. Kirmani, A. Breindel, R. Sheng, M. B. Maple, M. Dzero, and C. C. Almasan. "Non-kramers doublets and quest for the 'hidden-order' state in $PrNi_2Cd_{20}$ and $PrPd_2Cd_{20}$," *arXiv* (2020)

25. Yoichi Ando. "Topological insulator materials," *Journal of the Physical Society of Japan* **82**, 102001 (2013), DOI: https://doi.org/10.7566/JPSJ.82.102001

26. O. J. Schumann. "CLIP," (2009), http://clip4.sourceforge.net/.

27. M. M. Altarawneh, C. H. Mielke, and J. S. Brooks. "Proximity detector circuits: An alternative to tunnel diode oscillators for contactless measurements in pulsed magnetic field environments," *Review of Scientific Instruments* **80**, 066104 (2009), DOI: https://doi.org/10.1063/1.3152219

28. S. Ghannadzadeh, M. Coak, I. Franke, P. A. Goddard, J. Singleton, and J. L. Manson. "Measurement of magnetic susceptibility in pulsed magnetic fields using a proximity detector oscillator," *Review of Scientific Instruments* **82**, 113902 (2011), DOI: https://doi.org/10.1063/1.3653395

29. Hitoshi Sugawara, Yukihiro Abe, Yuji Aoki, Hideyuki Sato, Masato Hedo, Rikio Settai, Yoshichika Ōnuki, and Hisatomo Harima. "The fermi surface in filled skutterudite $RFe_4P_{12}$(R = La and Nd)," *Journal of the Physical Society of Japan* **69**, 2938-2946 (2000), DOI: https://doi.org/10.1143/JPSJ.69.2938

30. Tomoya Kubo, Eiich Matsuoka, Hisashi Kotegawa, Hideki Tou, Ai Nakamura, Dai Aoki, Hisatomo Harima, and Hitoshi Sugawara. "Fermi surface of the heavy-fermion

superconductor $PrTi_2Al_{20}$," *Journal of the Physical Society of Japan* **89**, 084704 (2020), DOI: https://doi.org/10.7566/JPSJ.89.084704

31. Neven Barišić, Sven Badoux, Mun K. Chan, Chelsey Dorow, Wojciech Tabis, Baptiste Vignolle, Guichuan Yu, Jérôme Béard, Xudong Zhao, Cyril Proust, and Martin Greven. "Universal quantum oscillations in the underdoped cuprate superconductors," *Nature Physics* **9,** 761 (2013), DOI: https://doi.org/10.1038/nphys2792

## Chapter 4: Magnetostriction of $URu_{2-x}Fe_xSi_2$ in High Magnetic Fields

### Introduction

$URu_2Si_2$ is a compound which has received much attention over several decades of study, mainly due to its hidden order phase [1]. At around 17.5 K, there is a large jump in the specific heat, indicating a phase transition [2, 3, 4]. However, the entropy change associated with this phase transition has not been associated with a corresponding order parameter in this material [1]. The entropy change is too large to be accounted for by the small moment antiferromagnetism that is sometimes observed to accompany this phase [1]. The phase it enters has thus been called the "hidden order" phase due to the uncertainty in the identity of its order parameter. The compound also exhibits unconventional superconductivity at around 1.2 K [1, 2, 3, 4]. There is also speculation that this superconductivity is topological in nature, which could suggest the existence of Majorana fermions, which could have applications in quantum computing [5, 6].

Under pressure, the hidden order undergoes a transition into a bulk anitferromagnetic phase, which appears upon suppression of the superconducting phase. Also, under pressure, there is a moderate increase in the hidden order transition temperature [7].

The Fe substituted $URu_2Si_2$ phase diagram is very similar to the behavior of $URu_2Si_2$ under pressure [8]. Indeed, as one would expect, the crystal structure decreases in volume due to the smaller iron atoms, and this can be mapped to an effective chemical pressure [9]. The hidden order transition temperature $T_o$ of Fe substituted $URu_2Si_2$ increases with Fe concentration, with a kink that mimics the kink in the $T_o$ vs $P$ diagram, suggesting a phase transition from hidden order to antiferromagnetism [9]. Because of this, Fe substituted $URu_2Si_2$ offers a real advantage in that the high pressure behavior of the sample can be studied at ambient pressure, allowing a variety

of techniques to be performed that would otherwise not be possible. One such method is magnetostriction.

High field magnetostriction measurements have been successfully carried out on $URu_2Si_2$, and allowed exploration of the high field phase diagram [10]. Signatures that were associated with the hidden order and other high field phases were observed, taking the form of a phase transition "dome" in the phase diagram around a quantum critical point as frequently shows up in heavy fermion behavior [10]. A natural continuation of this research, then, is to perform magnetostriction measurements using chemical doping with iron to attempt to similarly explore the three dimensional phase diagram.

**Experimental Procedure**

Single crystals of $URu_{2-x}Fe_xSi_2$ were grown using a tetra arc Czochralski growth method. Samples were shaped into small bars using an electrical discharge machine. The magnetostriction experiments were performed at the National High Magnetic Field Laboratory, Los Alamos National Laboratory, in pulsed magnetic fields at several temperatures. The samples were attached to an optical fiber using GE varnish, and the magnetostriction was measured based on reflections in the gratings inside the fiber as described in ref. [11]. As the sample contracts or expands, the grating also does so, and thus the wavelength of the reflected light shifts [11]. Samples were oriented with the c-axis parallel to the magnetic field.

**Results and Discussion**

Figure 4-1 (a) shows typical results from a magnetostriction measurement. Phase transitions in the samples can be observed as peaks in the 2nd derivative of the smoothed data as shown in figure 4-1 (b).

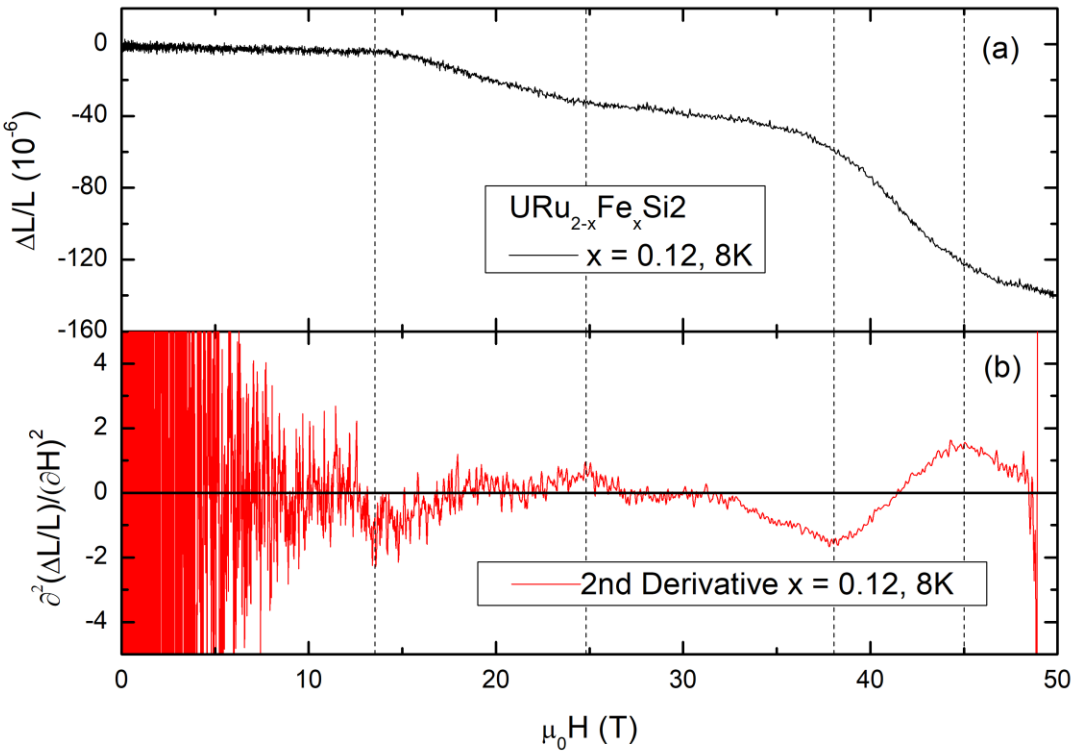


**Figure 4-1**(a) Example of magnetostriction data for $\Delta L/L$ vs $H$ for $URu_{2-x}Fe_xSi_2$, x = 0.12, at 8 K. (b) 2nd derivative of the magnetostriction data in (a) for $URu_{2-x}Fe_xSi_2$, x = 0.12, at 8 K. Dotted lines show the peaks and troughs in the 2nd derivative and how they correspond to points in the data. These points indicate the occurrence of phase transitions.

Figure 4-2 shows phase diagrams constructed from these transitions at various temperatures for different Fe concentrations of $URu_{2-x}Fe_xSi_2$. These can be compared to previous data from ref. [12], which mapped out the phase transitions in the $URu_{2-x}Fe_xSi_2$ system based on resistivity data. Figure 4-3 compares these data, and we can see that the magnetostriction data roughly corroborates the resistivity data. Interestingly, the hidden order transition is not evident at all in the magnetostriction data. This is in contrast to ref. [10], where hidden order was observed in pure $URu_2Si_2$ using magnetostriction. However the marker used in that paper for the hidden order was extremely subtle. It is also noteworthy that thermal expansion data shows that

the c-axis thermal expansion of $URu_2Si_2$ systems is very subtle [8]. It is possible that due to the pulsed nature of the magnetic fields employed in this study, the resulting noise in the magnetostriction obscured the marker in the data. This is plausible because the prior magnetostriction data were taken with static fields, rather than pulsed fields [10].

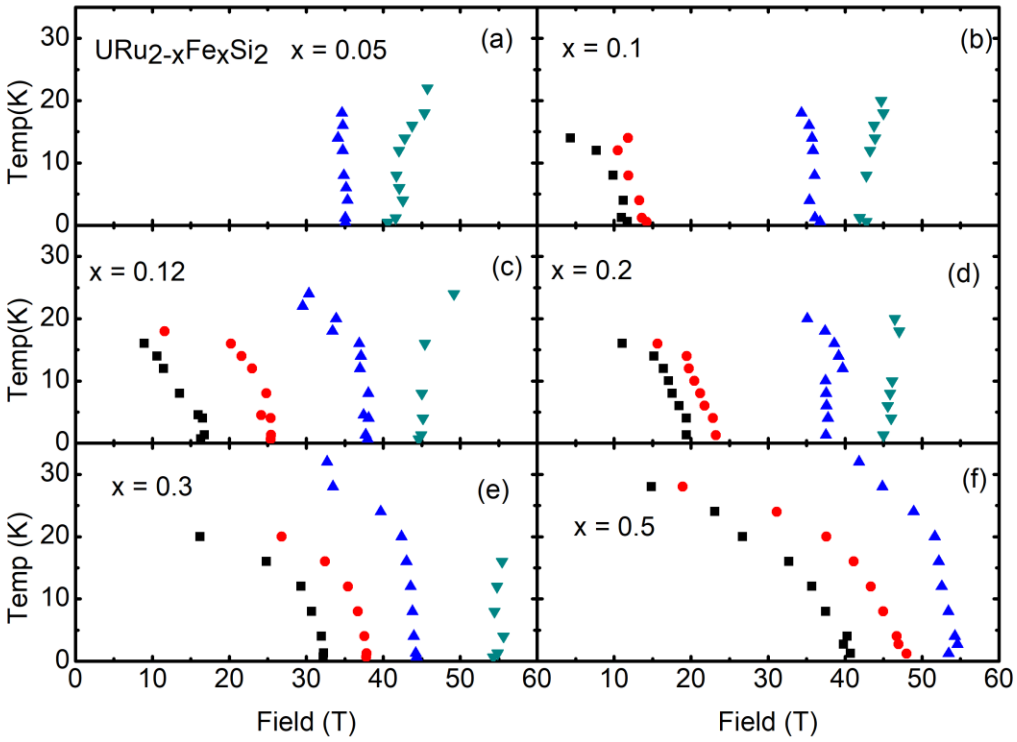


**Figure 4-2** Temperature vs. magnetic field phase diagrams for different values of x in $URu_{2-x}Fe_xSi_2$. The points indicate phase transitions as discussed in 4-1.

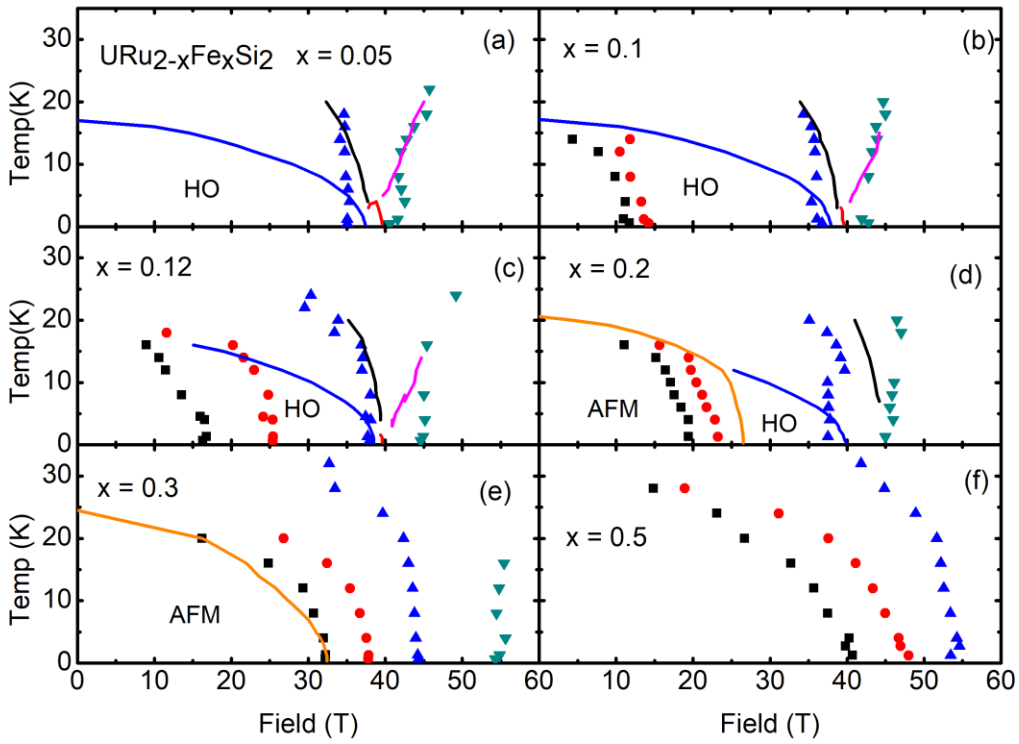


**Figure 4-3** Phase diagram as in figure 4-2 (solid symbols) compared to the phase diagrams from ref. [12] (lines). There is good agreement between the closed upward blue triangles and the black lines which in the literature match a broad maximum in the resistivity, which may indicate a metamagnetic quantum phase transition [12]. There is also good agreement between the closed downward teal triangles and the pink lines, which indicate a return to the normal metallic phase [12, 13]. Both the closed black squares and closed red circles roughly correspond to the orange lines which show the LMAF transition [12]. Clear signatures of neither the SDW and hidden order phases (red lines and blue lines) are not present in the data [12]. The possible metamagnetic transition and transition returning to a normal metallic phase both seem to have a kink at lower temperatures, which may be consistent with additional phases being present which are not directly apparent in the data, such as those suggested in ref. [13], possibly indicative of quantum criticality.

Other differences between the data in this study and the data in ref. [12] are in the precise location of some of the transitions. The antiferromagnetic transition can be affected by impurities [14]. These data also expand the phase diagram to higher fields and higher Fe concentrations and show that the antiferromagnetic order grows out of the hidden order phase as the field increases.

One thing that should be considered when performing high field measurements on $URu_2Si_2$ compounds is the impact of the magnetocaloric effect [15]. This effect alters the temperature of the compound in response to a magnetic field. One might suggest that the data are shifted in temperature from their true values by the magnetocaloric effect, and this explains the missing hidden order signature: that actually, rather than a different signature, what is indicated by the blue data points is a shifted hidden order signal. However, if one compares the apparent temperature shifts from the magnetocaloric effect in the parent compound $URu_2Si_2$ [15], with the required shifts in temperature for this explanation, one sees the required shifts are an order of magnitude greater than those observed in the parent compound reported in the literature, as is shown in figure 4-4. Further research on the magnetocaloric effect in the iron substituted $URu_2Si_2$ samples is needed. However, this comparison suggests that the magnetocaloric effect does not explain the invisibility of the hidden order to the magnetostriction probe.

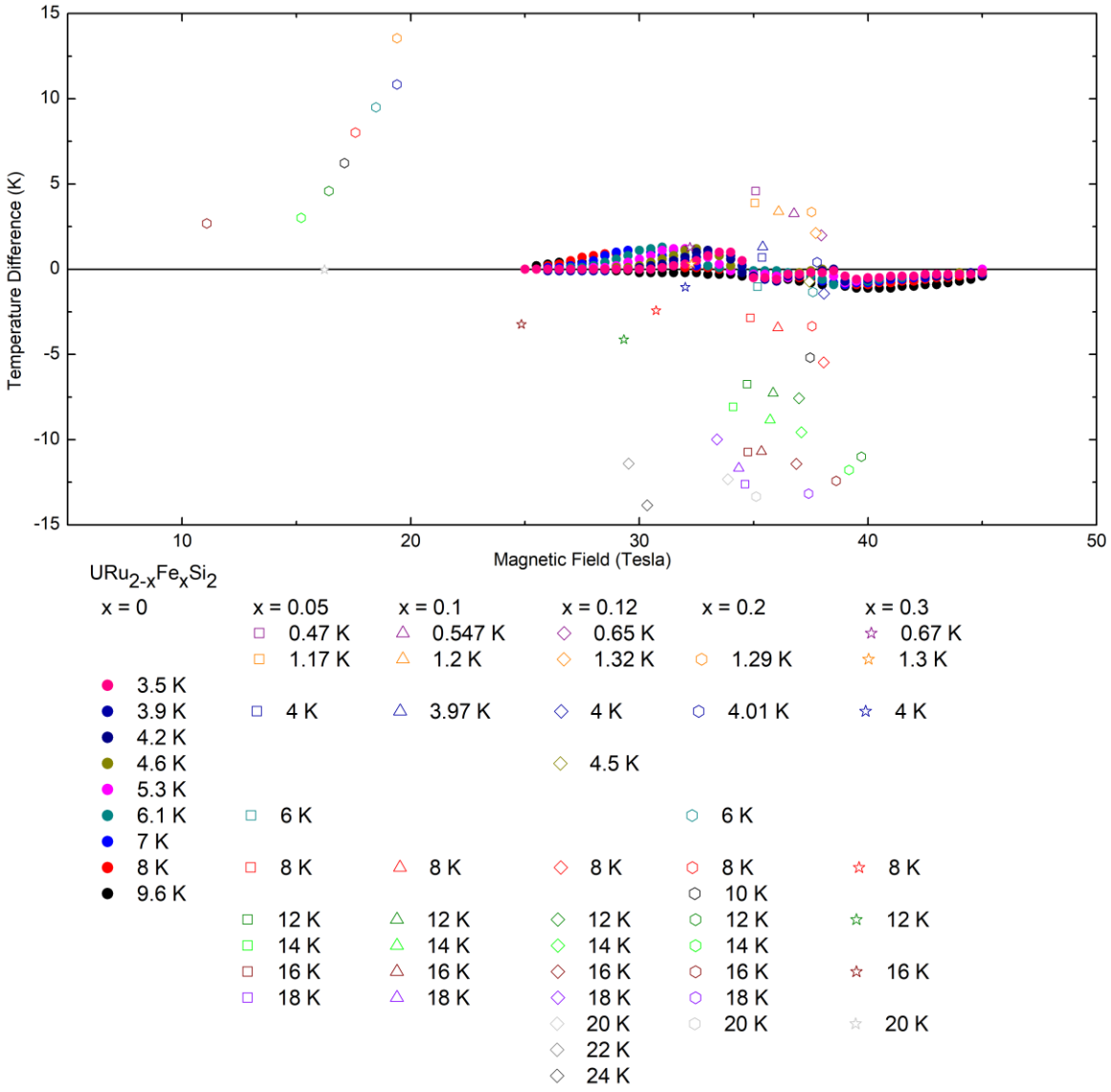


**Figure 4-4** Graph of temperature differences computed directly based on magnetocaloric effect data from ref. [15] for the parent compound, where each temperature value has been subtracted from the temperature at 25 T (solid points), compared with the necessary differences to explain the data as shifted from the values for either hidden order or antiferromagnetic transitions given in ref. [12] (open points). To aid in the comparison, the legend has been arranged as a table. It is clear that the shifting necessary is of an order of magnitude greater than the adjustments seen for the parent compound in the literature.

**Acknowledgements**

The National High Magnetic Field Laboratory is supported by the National Science Foundation through NSF/DMR-1157490/1644779 and the State of Florida. Research at UCSD

was supported by the US DOE BES under Grant No. DE-FG02-04-ER46105 (materials synthesis and characterization), the US NSF under Grant No. DMR-1206553 (low temperature measurements), and the NNSA under the SSAA program through the US DOE under Grant No. DE-NA0002909 (high field measurements) This research is also funded by a QuantEmX grant from ICAM and the Gordon and Betty Moore Foundation through Grant GBMF5305 to Alexander Breindel

Chapter 4, in full, is currently being prepared for submission for publication of the material. Ran, Sheng; Pouse, Naveen; Jeon, Inho; Jaime, Marcelo; Maple, M. Brian. The dissertation author was the primary investigator and author of this material.

## Bibliography


1. J. A. Mydosh and P. M. Oppeneer. "Colloquium: Hidden order, Superconductivity, and magnetism: The unsolved case of $URu_2Si_2$," *Rev. Mod. Phys.* **83,** 1301-1322 (2011), DOI: http://dx.doi.org/10.1103/RevModPhys.83.1301

2. M. B. Maple, J. W. Chen, Y. Dalichaouch, T. Kohara, C. Rossel, M. S. Torikachvili, M. W. McElfresh, and J. D. Thompson. "Partially gapped Fermi surface in the heavy-electron superconductor $URu_2Si_2$," *Phys. Rev. Lett.* **56,** 185 (1986), DOI: https://doi.org/10.1103/PhysRevLett.56.185

3. T. T. M. Palstra, A. A. Menovsky, J. van den Berg, A. J. Dirkmaat, P. H. Kes, G. J. Nieuwenhuys, and J. A. Mydosh. "Superconducting and magnetic transitions in the heavy-fermion system $URu_2Si_2$," *Phys. Rev. Lett.* **55**, 2727-2730 (1985), DOI: https://doi.org/10.1103/PhysRevLett.55.2727

4. W. Schlabitz, J. Baumann, B. Pollit, U. Rauchschwalbe, H. M. Mayer, U. Ahlheim, and C. D. Bredl, "Superconductivity and magnetic order in a strongly interacting Fermi-system: $URu_2Si_2$," *Z. Phys. B Condens. Matter* **62,** 171 (1986), DOI: https://doi.org/10.1007/978-94-011-1622-0_9

5. Tanmoy Das. "Weyl semimetal and superconductor designed in an orbital-selective superlattice." *Phys. Rev. B* **88**, 035444 (2013), DOI: http://dx.doi.org/10.1103/PhysRevB.88.035444

6. Tanmoy Das. "Spin-orbit density wave induced hidden topological order in$URu_2Si_2$," *Scientific Reports* **2**, 596 (2012), DOI: https://doi.org/10.1038/srep00596

7. Nicholas P. Butch, Jason R. Jeffries, Songxue Chi, Juscelino Batista Leão, Jeffrey W. Lynn, and M. Brian Maple. "Antiferromagnetic critical pressure in $URu_2Si_2$ under hydrostatic conditions," *Phys. Rev. B* **82**, 060408 (2010), DOI: https://doi.org/10.1103/PhysRevB.82.060408

8. Sheng Ran, Christian T. Wolowiec, Inho Jeon, Naveen Pouse, Noravee Kanchanavatee, Benjamin D. White, Kevin Huang, Dinesh Martien, Tyler DaPron, David Snow, Mark Williamsen, Stefano Spagna, Peter S. Riseborough, and M. Brian Maple. Phase diagram and thermal expansion measurements on the system $URu_{2-x}Fe_xSi_2$," *Proceedings of the National Academy of Sciences* **113**, 13348-13353 (2016), DOI: https://doi.org/10.1073/pnas.1616542113

9. N. Kanchanavatee, M. Janoschek, R. E. Baumbach, J. J. Hamlin, D. A. Zocco, K. Huang, and M. B. Maple. "Twofold enhancement of the hidden-order/large-moment antiferromagnetic phase boundary in the $URu_{2-x}Fe_xSi_2$ system," *Phys. Rev. B* **84**, 245122 (2011), DOI: https://doi.org/10.1103/PhysRevB.84.245122

10. V. F. Correa, S. Francoual, M. Jaime, N. Harrison, T. P. Murphy, E. C. Palm, S. W. Tozer, A. H. Lacerda, P. A. Sharma, and J. A. Mydosh. "High-magnetic-field lattice length changes in $URu_2Si_2$," *Phys. Rev. Lett.* **109**, 246405 (2012), DOI: http://dx.doi.org/10.1103/PhysRevLett.109.246405

11. Marcelo Jaime, Carolina Corvalán Moya, Franziska Weickert, Vivien Zapf, Fedor F. Balakirev, Mark Wartenbe, Priscila F. S. Rosa, Jonathan B. Betts, George Rodriguez, Scott A. Crooker, and Ramzy Daou. "Fiber Bragg grating dilatometry in extreme magnetic field and cryogenic conditions," *Sensors* **17**, 2572 (2017), DOI: https://doi.org/10.3390/s17112572

12. Sheng Ran, Inho Jeon, Naveen Pouse, Alexander J. Breindel, Noravee Kanchanavatee, Kevin Huang, Andrew Gallagher, Kuan-Wen Chen, David Graf, Ryan E. Baumbach, John Singleton, and M. Brian Maple. "Phase diagram of $URu_{2-x}Fe_xSi_2$ in high magnetic fields," *Proceedings of the National Academy of Sciences* **114**, 9826-9831 (2017), DOI: https://doi.org/10.1073/pnas.1710192114

13. K. H. Kim, N. Harrison, M. Jaime, G. S. Boebinger, and J. A. Mydosh. "Magnetic-field-induced quantum critical point and competing order parameters in $URu_2Si_2$," *Phys. Rev. Lett.* **91**, 256401 (2003), DOI: https://doi.org/10.1103/PhysRevLett.91.256401

14. Shigeru Takagi, Shu Ishihara, Satoru Saitoh, Hiko-ichiro Sasaki, Hiroshi Tanida, Makoto Yokoyama, and Hiroshi Amitsuka. "No evidence for "small-moment antiferromagnetism" under ambient pressure in $URu_2Si_2$: Single-crystal $^{29}Si$ NMR study," *Journal of the Physical Society of Japan* **76**, 033708 (2007), DOI: https://doi.org/10.1143/JPSJ.76.033708

15. M. Jaime, K. H. Kim, G. Jorge, S. McCall, and J. A. Mydosh. "High magnetic field studies of the hidden order transition in $URu_2Si_2$," *Phys. Rev. Lett.* **89**, 287201 (2002), DOI: https://doi.org/10.1103/PhysRevLett.89.287201

## Chapter 5: High magnetic field and high pressure transport properties of the conducting surface state of FeSi and its comparison with $SmB_6$


### Abstract

The recent discovery of a conducting surface state in FeSi has suggested the possibility of topological behavior [1]. In this work, we further explore this conducting surface state using magnetoresistance measurements in high magnetic fields up to 60 T, electrical resistivity measurements at high pressures up to 7.6 GPa, as well as magnetic field modulated microwave spectroscopy (MFMMS). The two energy gaps of FeSi determined from the temperature dependence of electrical resistance increased with pressure up to about 7 GPa, followed by a drop which coincides with a sharp suppression on the conducting surface transition temperature. The closing of the energy gaps with pressure was also seen in the Kondo insulator $SmB_6$ [2], a suspected topological Kondo insulator. The magnetoresistance behavior shows additional evidence for a conducting surface state by comparing the behavior perpendicular and parallel to the applied magnetic field. Comparisons of the magnetoresistance of FeSi and $SmB_6$ show similar behaviors. However, the MFMMS results presented here suggests there are differences in the underlying physics of the surface state in these two compounds.


### Introduction

The transition metal silicide FeSi is of great interest for both its unique electrical transport and magnetic properties and its behavior as a *d*-electron analogue to an *f*-electron Kondo insulator. The low-temperature electrical resistivity reveals a crossover from semiconducting behavior to metallic behavior, the emergence of a conducting surface state, and a linear dependence of the electrical resistivity on sample width in the metallic phase as shown in

Figure 5-1 [1]. Other materials such as the first discovered Kondo insulators samarium hexaboride ($SmB_6$) and golden phase of samarium monosulfide (SmS) share similar properties [3]. $SmB_6$ is also believed to be a topological Kondo insulator [4, 5]. Topological materials have gained much attention recently owing to the possibility that topological superconductors act as hosts for Majorana fermion quasiparticles, which have applications in quantum computing error correction. [6].

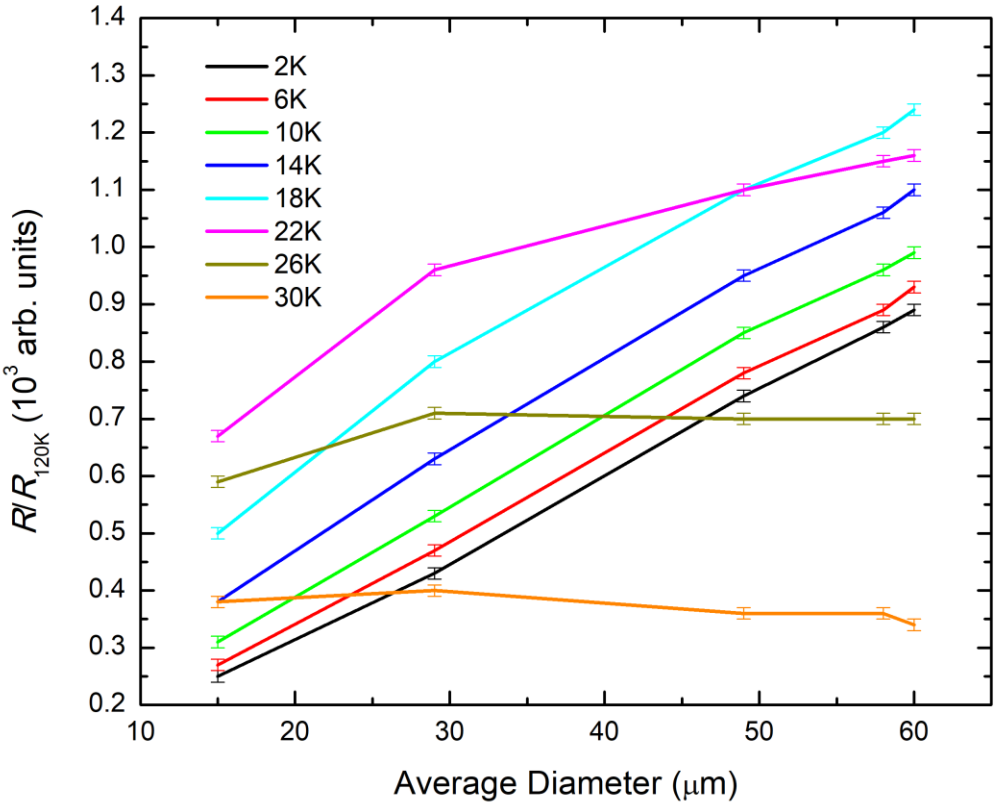


**Figure 5-1** Electrical resistance R, normalized to its value at 120 K, vs the average diameter of and approximately cylindrical rod shaped sample of FeSi, from the data reported in [1] (taken by using data thief software [7]). Error bars are included to account for errors in the data retrieval. The linearity of the plots suggests the formation of a conducting surface state below around 19 K, because of the increased surface area to volume ratio associated with thinning the samples [1].

The temperature T dependence of the electrical resistance R of the high quality single crystals of FeSi obeys a standard activation model with a two-gap feature at higher temperatures and metallic behavior appearing below 19 K [1]. The observation that the normalized $R$ ($T$) below 19 K shows a dependence on the dimensions of FeSi specimens and the absence of an anomaly in the specific heat at 19 K indicate the existence of a conducting surface state [1]. A conducting surface state is also observed in $SmB_6$ below 5 K [8]. The similarities between FeSi and $SmB_6$ suggest that FeSi may be a topological Kondo insulator. Recent research employing scanning tunneling microscopy on high quality FeSi single crystals support the existence of surface conductivity of the material and the comparison to $SmB_6$ [9]. This paper will present a comparison between FeSi and $SmB_6$ using electrical resistivity at ambient and high magnetic fields, as well as magnetic field modulated microwave spectroscopy (MFMMS). Additionally, high pressure measurements on FeSi are used to further explore the behavior of the surface state.

**Experimental Procedure**

The FeSi single crystals were prepared using flux growth methods as described in ref. [1]. $SmB_6$ samples were grown in an aluminum flux [10]. Magnetoresistance measurements were carried out at Los Alamos National High Magnetic Field Laboratory (NHMFL) in pulsed fields up to 60 T at temperatures from 0.7 K to 27 K. Electrical resistance measurements at ambient pressure were performed at the University of California San Diego (UC San Diego) in a Quantum Design PPMS DynaCool at temperatures down to 1.8 K. The measurements of electrical resistivity under pressure were carried out at the Center for High Pressure Science and Technology Advanced Research in Shanghai with a diamond anvil cell (DAC) and at the University of California, San Diego with a hydrostatic piston cylinder cell (PCC).

High pressure is a powerful tool for tuning atomic distances, resulting in fundamental changes in electronic structure. For example, pressure can alter the magnitude of the negative covalent mixing exchange coupling constant between conduction- and localized *f*-electron spins and thus increase and then decrease the ordering temperatures of lanthanide elements (Nd, Sm, Tb, Dy) [11]. Pressure also induces or increases the overlap between 4 *f* or 5*f* magnetic moments in heavy fermion materials, resulting in complex phase diagrams [12].

A single crystalline FeSi sample (bar shape, 25 μm thick and 80 μm long) was compressed to a maximum pressure of 7.6 GPa in a DAC using diamond anvils each with a culet size of 300 micrometers. A 300 μm thick beryllium gasket was pre-indented to 48 μm with a 150-μm-diameter hole laser drilled through the center of the pre-indentation area. A cubic boron nitride (cBN) insulating layer was compressed onto the surface of the gasket. The laser was used again to make a new hole in the cBN layer. The hole was then filled with sodium chloride (NaCl) which served as a good pressure transmitting medium. Several ruby spheres were placed within the NaCl pressure transmitting medium, serving as the pressure gauge. A standard four-point method was used to measure the resistance of the sample under pressure with platinum strips as the electrical leads. An AC resistance bridge was used with an amplitude from 0.01 to 0.1 mA, 22 or 33 Hz excitation current. The DAC containing the sample was inserted into a cryostat capable of varying temperature from 300 K to 2 K and magnetic field from 0 T to 3 T. Pressures were determined at room temperature.

A PCC made of nonmagnetic materials was used for measuring the electrical resistivity of FeSi under hydrostatic pressures up to 2.45 GPa. A piece of single crystalline FeSi was placed in a Teflon capsule filled with a liquid pressure-transmitting medium composed of a mixture of n-pentane and isoamyl alcohol (volume ratio 1:1). Mutual inductance coils embedded within the

BeCu clamp body were used to measure the ac magnetic susceptibility of a tin or lead superconducting manometer inside the sample space from which the superconducting critical temperature and, in turn, the pressure was determined. An LR 700 AC resistance bridge was employed to measure the electrical resistance of the sample. A liquid helium dewar was used to vary the temperature of the sample from room temperature to 1.5 K by adjusting the height of the pressure clamp above the liquid helium bath and by pumping on the liquid helium bath after the clamp was immersed in the liquid.

Single crystal samples of FeSi and $SmB_6$ were measured for surface transitions using a magnetic field modulated microwave spectroscopy (MFMMS) technique (see Ref. [13]). The MFMMS setup consists of a customized Bruker X-band (9.4 GHz) electron paramagnetic resonance (EPR) apparatus including a microwave power source, a dual-mode cavity resonator, lock-in detector, and a 1 T electromagnet.

The MFMMS technique measures the reflected microwave power from a sample as a function of temperature [13]. In general, the absorption of microwave power depends on the surface resistance of a material. For example, when a material undergoes a superconducting transition, the decrease in surface resistance reduces the absorption of microwave power at the surface. Near the superconducting transition, there is a pronounced peak in the MFMMS signal.

Five rod-like single crystal FeSi samples were placed at the bottom of a thin quartz tube which was then flushed with helium gas and sealed with paraffin film. Individual $SmB_6$ single crystal samples were similarly sealed in quartz tubes. The FeS and $SmB_6$ samples in the bottom of the quartz tubes were then placed at the center of a cavity resonator where the magnetic field

component of the $TE_{102}$ mode is at a maximum. The five needle-like FeSi crystals had lengths ranging from 1.15 to 1.9 mm and diameters ranging from 45 to 60 micrometers.

Field cooled (FC) measurements were performed at various DC fields set with the electromagnet while the sample temperature was swept at a rate of 1 K per minute using an Oxford helium flow cryostat and temperature control. The application of an external ac magnetic field of 15 Oe at 100 KHz and the use of a lock-in amplifier provided an enhanced signal and reduction of noise for the detection of reflected microwave power. All MFMMS measurements of both FeSi and $SmB_6$ samples were performed at a microwave power of 1 mW.

**Results and Discussion**

Figure 5-2 shows the transverse magnetoresistance $R_{\perp}$ for single crystalline FeSi specimen as a function of magnetic field H at various temperatures between T = 0.7 K and 27 K. The resistance measurements reveal a maximum $R_{\perp}$ at 20 K, as can be seen more clearly in Fig. 5-3, near the temperature $T_S$ below which the conducting surface state forms [1]. As the temperature is lowered, the field required to drive the system out of the conducting surface state increases. The inset of Fig. 5-2 shows $T_S$ as a function of temperature and magnetic field.

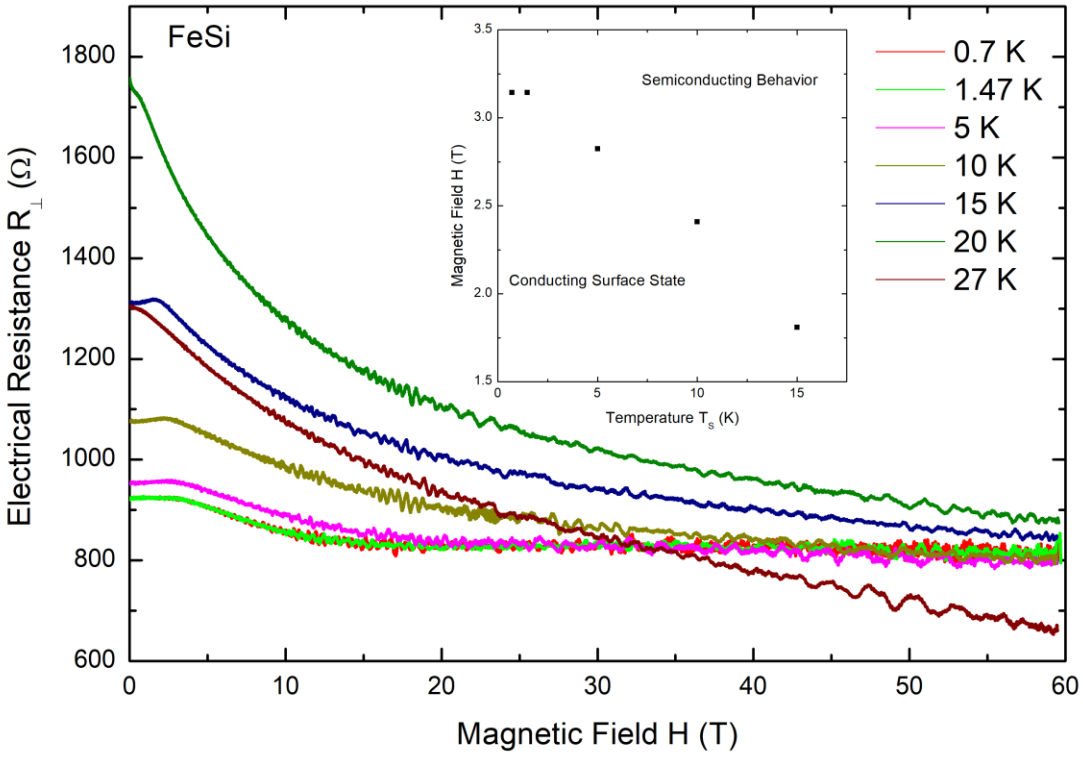


**Figure 5-2** Transverse magnetoresistance $R_{\perp}$ as a function of magnetic field H at various temperatures between T = 0.7 K and 27 K. The measurements were performed upon field downsweep. Inset: Plot of H vs. $T_S$ showing the suppression of $T_S$ with increasing field. Black points correspond to the peaks in the electrical resistivity at the transition from semiconducting to metallic behavior of the surface state.

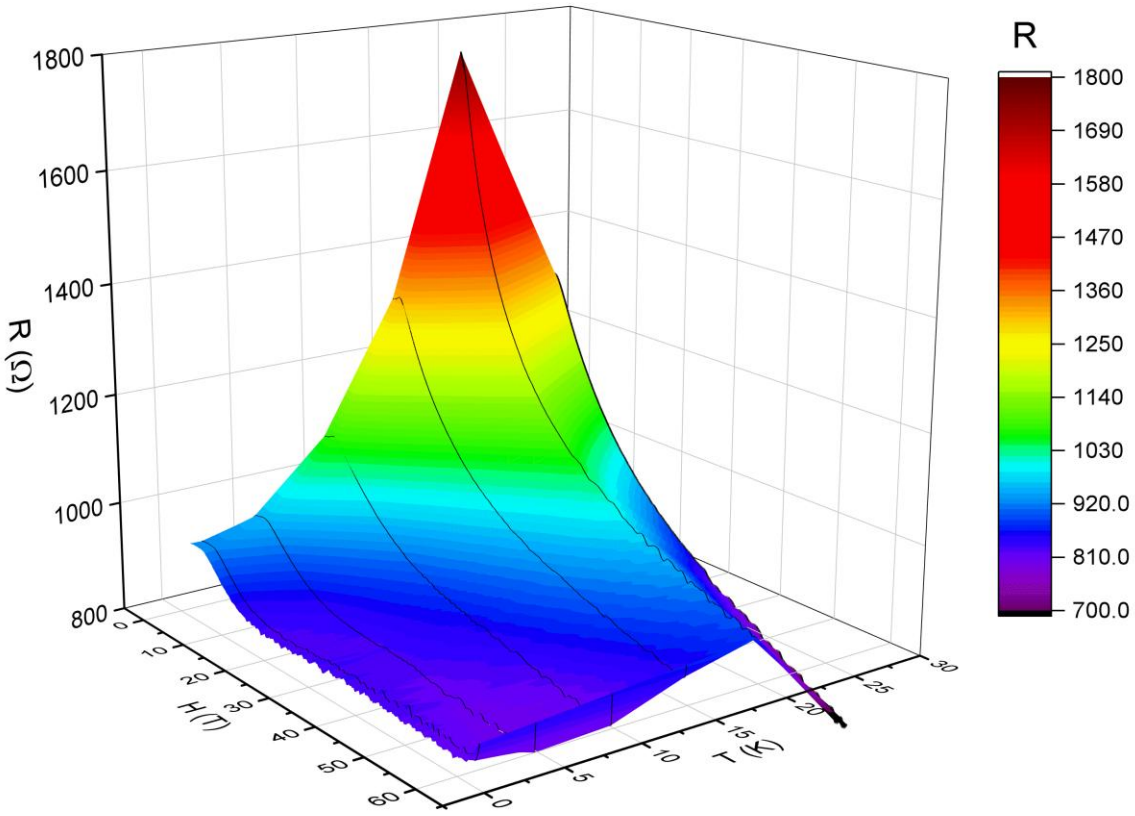


**Figure 5-3** 3D surface plot derived from the magnetoresistance $R_{\perp}$ vs. magnetic field H and temperature T data shown in Figure 5-2. There is a clear peak in the $R_{\perp}(H, T)$ data around 20 K, associated with the transition to the conducting surface state [1].

The transverse magnetoresistance $R_{\perp}$ is compared with the longitudinal magnetoresistance $R_{\parallel}$ in Fig. 5-4 at temperatures below $T_S$. A schematic of the geometry of the magnetoresistance measurements is shown in the inset of Fig. 5-4 where the magnetic field is oriented perpendicular and parallel to the cylindrical axis of the sample. It is clear from the data in Fig. 5-4 that there is significant anisotropy in the magnetoresistance associated with the transition, despite the cubic crystal structure of FeSi [1]. These results are consistent with our previously published magnetoresistance data on FeSi samples, and, as explained in our previous

work, the difference caused by the change in field orientation can be understood as a consequence of a positive field response of the contribution of the surface conductivity to the overall magnetoresistance [1].

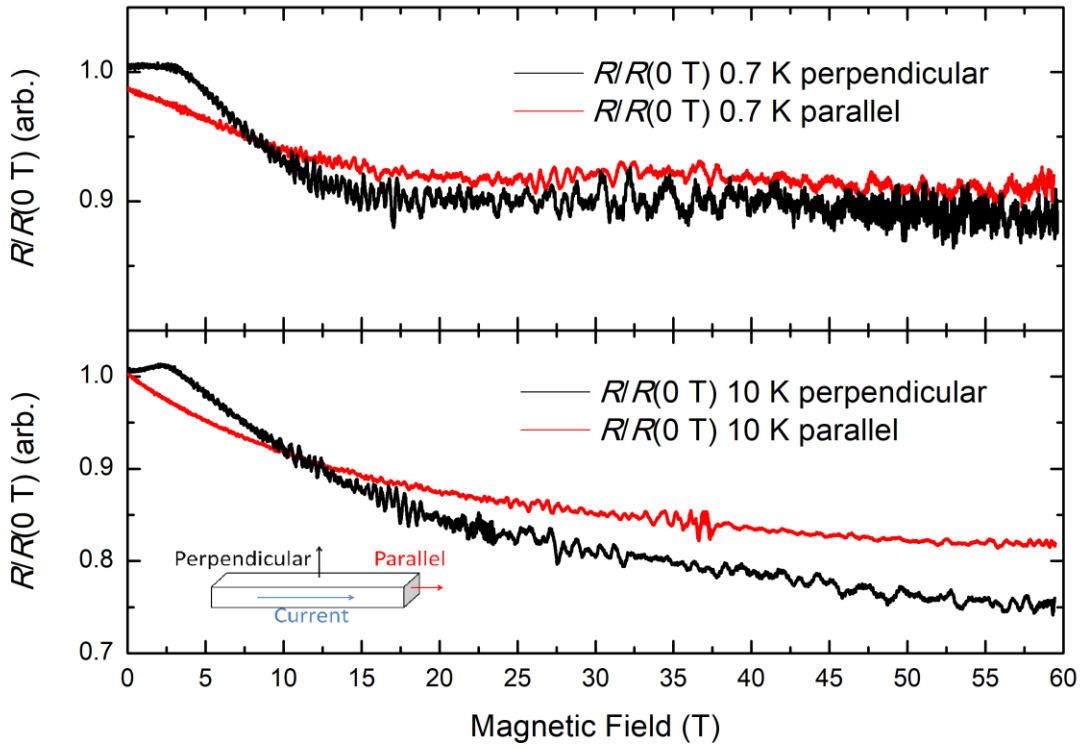


**Figure 5-4** The anisotropic magnetoresistance (AMR) at 0.7 K (top) and 10 K (bottom). The geometries used in the AMR measurements are shown in the inset. The current is directed along the longitudinal axis of the single crystal. The transverse magnetoresistance $R_{\perp}$ (black curves) was measured with the magnetic field perpendicular to the longitudinal axis of the FeSi single crystal. The longitudinal magnetoresistance $R_{\parallel}$ (red curves) was measured with the field parallel to the axis of the FeSi single crystal. The cylindrical axis of the FeSi single crystal corresponds to the [111] direction of the cubic crystal structure. The electrical resistance data R(H) are normalized to the value of R at H = 0 T.

Shown in Fig. 5-5 are temperature dependent resistance *R*(*T*) curves for FeSi from 2 K to room temperature at various pressures up to 7.6 GPa. There is a persistent peak in the resistance

around 20 K for all pressures except 7.6 GPa signifying the remarkable change in the transport behavior of FeSi at $T_S$. On the higher temperature side of the peak in $R$ ($T$), the FeSi sample exhibits semiconducting-like behavior with $\frac{dR}{dT} < 0$, whereas on the lower temperature side, the sample displays metallic behavior ($\frac{dR}{dT} > 0$). The same phenomenon has been observed at ambient pressure [1] and can be attributed to the emergence of the conducting surface state in FeSi below the temperature $T_S$ at which the peak in $R$($T$) occurs. As the pressure is increased to 7.6 GPa, the well-defined peak in $R$($T$) vanishes and the resistance of the sample continues to increase as $T$ is reduced to a base temperature of 2 K. This suggests the occurrence of a pressure-induced transition from metallic to insulating-like behavior of the surface state at this pressure. The B20 crystal structure of FeSi (ϵ-FeSi) is quite stable under high pressure. At room temperature, no phase transition was observed to at least 36 GPa. Even with laser heating to above 1000 K, the high-pressure B2 phase (CsCl type FeSi) persists to pressures at least above 14 GPa [14, 15]. Consequently, the pressure-induced change in $R$($T$) of FeSi at 7.6 GPa could be ascribed to an electronic phase transition, and independent of any structural transition.

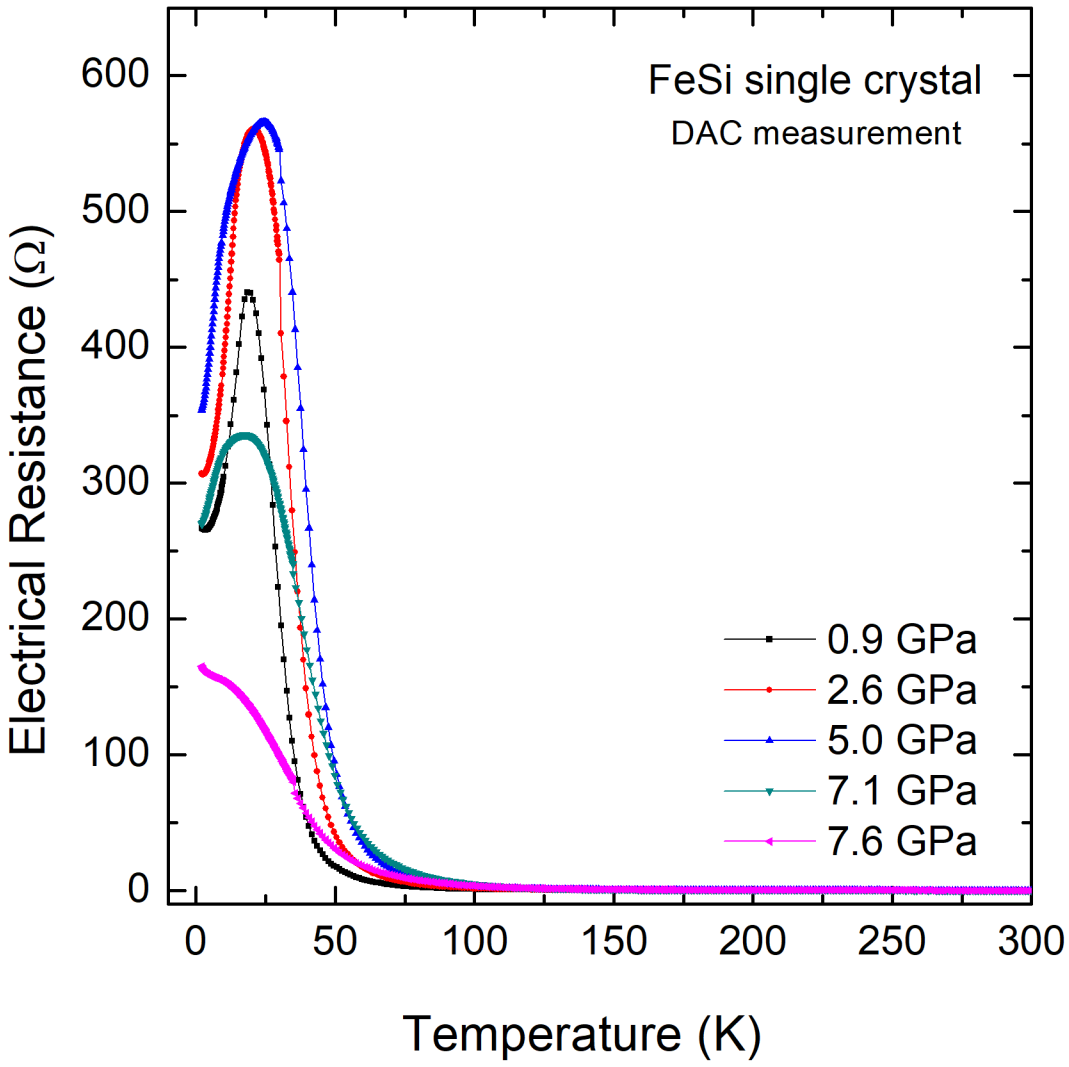


**Figure 5-5** Electrical resistance $R$ vs temperature $T$ for an FeSi single crystal at various pressures up to 7.6 GPa measured in DAC experiments.

FeSi has been proposed as a *d*-electron Kondo insulator [5]. For a Kondo insulator, a narrow hybridization gap (Kondo gap) develops below a characteristic temperature called the Kondo temperature ($T_K$), because of the coherent spin-dependent scattering of itinerant electrons by the lattice of *d*- or *f*-electron localized magnetic moments. This Kondo scenario is partly consistent with what we found for the $R(T)$ behavior of FeSi. As shown in Fig. 5-6, $T_K$ is defined as the temperature below which the resistance can be described by a gapped semiconducting activation model. The energy gap $\Delta$ has been extracted from an Arrhenius law,

$$R = R_o \exp(\Delta/2k_B T) \tag{5-1}$$

where $R_o$ is a constant. The energy gap $\Delta$ can be extracted from the slope of the linear portion of a plot of $\ln R$ vs $1/T$. This is illustrated in the $\ln R$ vs $1/T$ plot in Fig. 5-6 based on measurements of $R(T)$ for FeSi at 0.9 GPa. The linear region from 70 K to 160 K = $T_K$ corresponds to an energy gap $\Delta_1$ = 57 meV, while the linear region from 37 K to 57 K yields an energy gap $\Delta_2$ = 36 meV. Thus, at 0.9 GPa, FeSi evolves from a non-activated regime at $T_K$ = 160 K to a second regime where $R(T)$ is characterized by an energy gap $\Delta_1$ = 57 meV, then to a third regime characterized by a smaller energy gap $\Delta_2$= 36 meV, and finally to a fourth regime involving a conducting surface state below $T_S$ = 19 K.

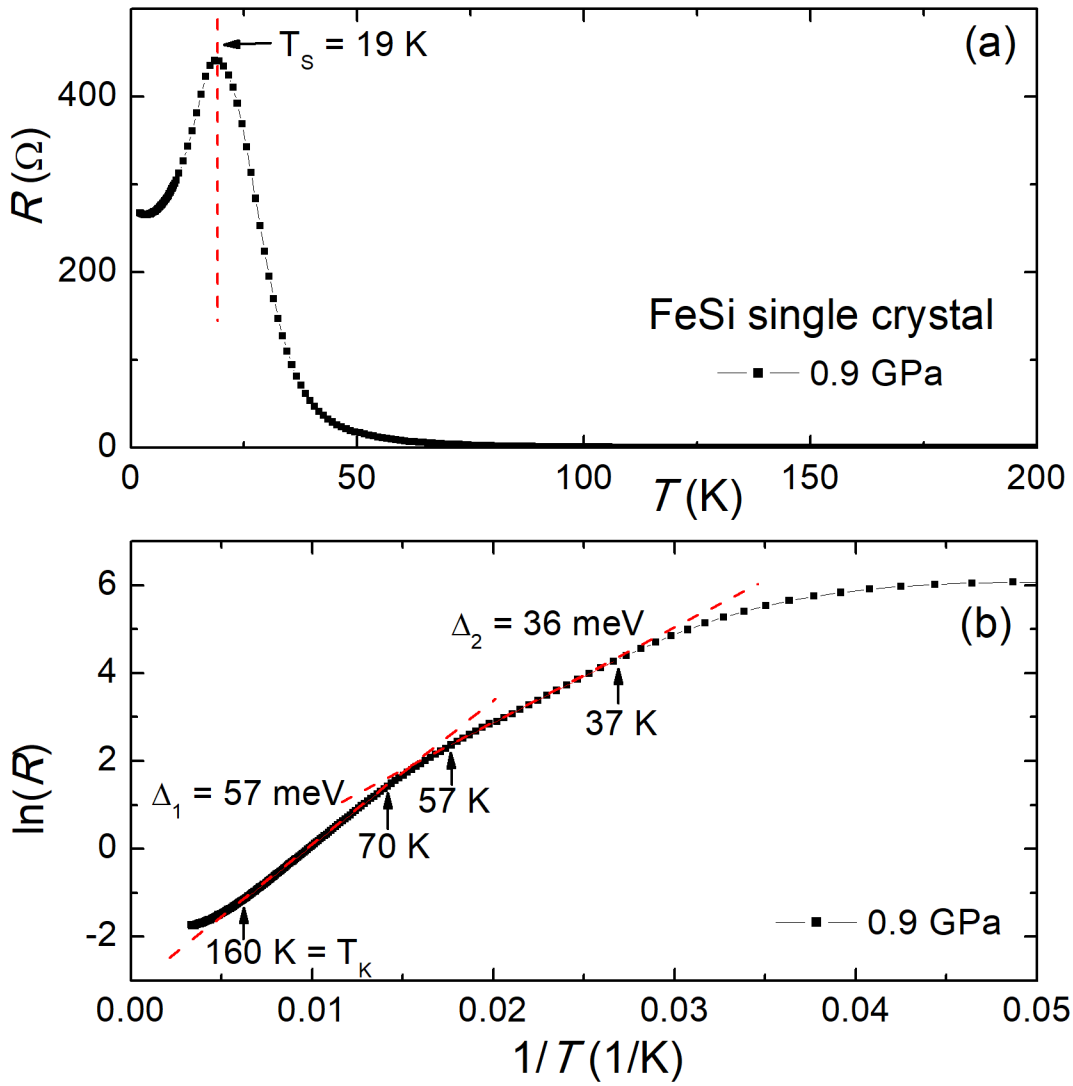


**Figure 5-6** (a) A representative plot of $R(T)$ at $P$ = 0.9 GPa illustrating the location of $T_S$ at the peak in $R(T)$ marked by the vertical dashed red line. (b) A plot of ln $R$ vs $1/T$ that allows for the extraction of the the energy gaps $\Delta_1$ (in the temperature range $T_K$ = 160 to 70K) and $\Delta_2$ (in the range $T$ = 57 to 37 K) according to an Arrhenius law. Within each region, $R(T)$ is fitted with an Arrhenius law (See Equation (5-1) and discussion in text.)

The same procedure was used to determine the two energy gaps $\Delta_1$ and $\Delta_2$ at different pressures based on $R(T)$ measurements performed in PCC and DAC experiments. The pressure dependence of both energy gaps are plotted in Figure 5-7 (a). The energy gaps initially increase with pressure and then begin to decrease around 7 GPa. Correspondingly, in Figure 5-5 it can be seen that the peak resistance also first increases and then decreases with increasing pressure, a

direct result from the change in the energy gaps under pressure. Furthermore, there is a correspondence of the suppression of the energy gap and the drop in $T_S$, indicated by the vertical dashed line in Figure 5-7. The closing of the energy gaps is correlated with the disappearance of the conducting surface state in FeSi. The pressure dependence of the Kondo temperature and the temperature $T_S$ of the onset of the conducting surface state $T_K(P)$ and $T_S$ ($P$) for the single crystalline FeSi sample are plotted in a $T$ vs $P$ phase diagram in Figure 5-7 (b). Above $T_K$, the sample can be characterized as a bad metal in which itinerant electrons are incoherently scattered by the *d*-electron localized magnetic moments, yielding a very high resistivity compared to that of a simple metal. Between $T_K$ and $T_S$, FeSi is expected to be a Kondo insulator, whereas below $T_S$, a conducting surface state appears, as discussed in our earlier publication [1].

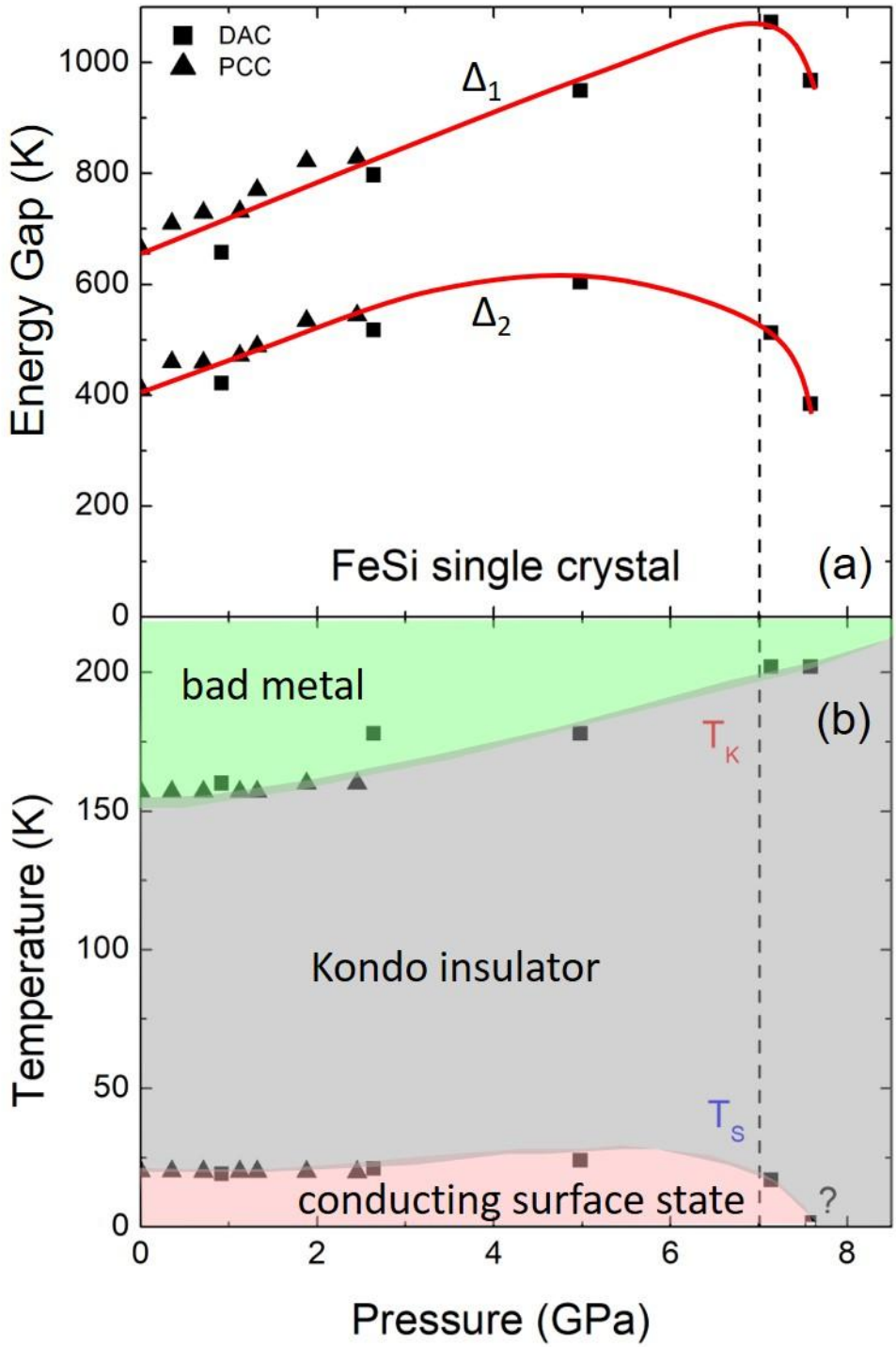


**Figure 5-7** (a) Evolution of the two energy gaps $\Delta_1$ and $\Delta_2$ with pressure obtained from electrical resistivity measurements in PCC and DAC experiments. (b) *T-P* phase diagram for the FeSi single crystal. The red lines in (a) and the boundaries between different phases are guides to the eye. The question mark indicates the estimation of $T_S$ at 7.6 GPa.

Since the proposal of a "topological Kondo insulator" in 2010 [4], the *f*-electron Kondo insulator $SmB_6$ was considered a prime candidate for a topological Kondo insulator. As a *d*-electron analog of $SmB_6$, FeSi shares many common attributes with $SmB_6$, including similar electrical transport properties at both ambient and high pressure. At ambient pressure, F. Chen *et al.* also observed two-gap-semiconducting behavior in high quality $SmB_6$ at intermediate temperatures and a conducting surface state below 5 K [8]. At high pressures, this study reveals that the energy gaps of FeSi increase with pressure before they start to fall above 7 GPa. Early in 1997, E. Bauer *et al.* [16] also reported a broadening of the energy gap of FeSi under pressures up to 1.3 GPa, with no indication of metallization even at 9.4 GPa. Extending the pressure range for FeSi is our future goal to determine the pressure at which the energy gaps vanish. The closure of the Kondo gap at similar critical pressures (4 – 7 GPa), accompanied by a fundamental change in $R(T)$ for $SmB_6$ has been reported by several groups [2, 17, 18]. Using the Anderson lattice model for a Kondo insulator, the indirect hybridization gap obtained by fitting the activation behavior of $R(T)$ is of the order of $V^2/D$, where $V$ is the hybridization energy between the localized *d*- or *f*- and conduction electron states and $D$ the half bandwidth of the conduction band. Both $V$ and $D$ are expected to increase asymptotically with decreasing inter-atomic distance with increasing pressure. This asymptotic behavior is complicated by the node in the Si 3*p* radial wave function and the angular dependence of the wave functions of atoms. A non-monotonic pressure dependence of the Kondo gap may appear because of this complication. At sufficiently high pressure, the hybridization and the hybridization gap would finally vanish, supported by the observations of the gap closure in $SmB_6$ and $Ce_3Bi_4Pt_3$ [19], two typical Kondo insulators. For FeSi, the scenario is even more complicated because the 3*d* state is less localized than the 4*f* state. It would be interesting to explore whether the gaps in FeSi under pressure

would finally collapse or not, since this might clarify the validity of the hybridization model for this *d*-electron analog of a Kondo insulator.

To gain further understanding of the transition to a surface conducting state in FeSi at 20 K, magnetic field modulated microwave spectroscopy (MFMMS) measurements were performed on single crystals of FeSi as a function of temperature from 4 K to 100 K in both zero field as well as in an applied DC magnetic field of 500 Oe, the results of which are shown in Figure 5-8. In zero field, there is a clear peak with an onset at approximately 19 K (see Figure 5-8(a)). At an applied DC magnetic field of 500 Oe, the main peak in MFMMS intensity has shifted to higher temperature with an onset at $T$ = 21 K (see Figure 5-8(b)). The peaks in the MFMMS signal observed for single crystalline FeSi are reminiscent of the large peaks observed at the onset of a superconducting transition, where the decrease in the surface resistivity during the superconducting transition is the cause for the spike in microwave absorption. The MFMMS signal for the FeSi samples are somewhat unexpected and remarkable for their correspondence to the insulating to metallic transition in the surface state at $T_S$ = 19 K. Previous MFMMS experiments on vanadium sesquioxide ($V_2O_3$), which exhibits a metal to insulator transition with a six order of magnitude change in electrical resistance upon cooling at 160 K, show no peak-like signature associated with the resistivity change [13]. This is the first occurrence of a superconducting-like peak in a MFMMS measurement for a sample that is not superconducting. The detection of this type of surface resistance change has not been previously reported in a MFMMS measurement. As a comparison, MFMMS measurements were also performed on two $SmB_6$ samples in zero applied DC field as shown in Figure 5-8 (b). Unlike FeSi, the $SmB_6$ MFMMS signal contained no signatures of any transition for 4 K < $T$ < 100 K.

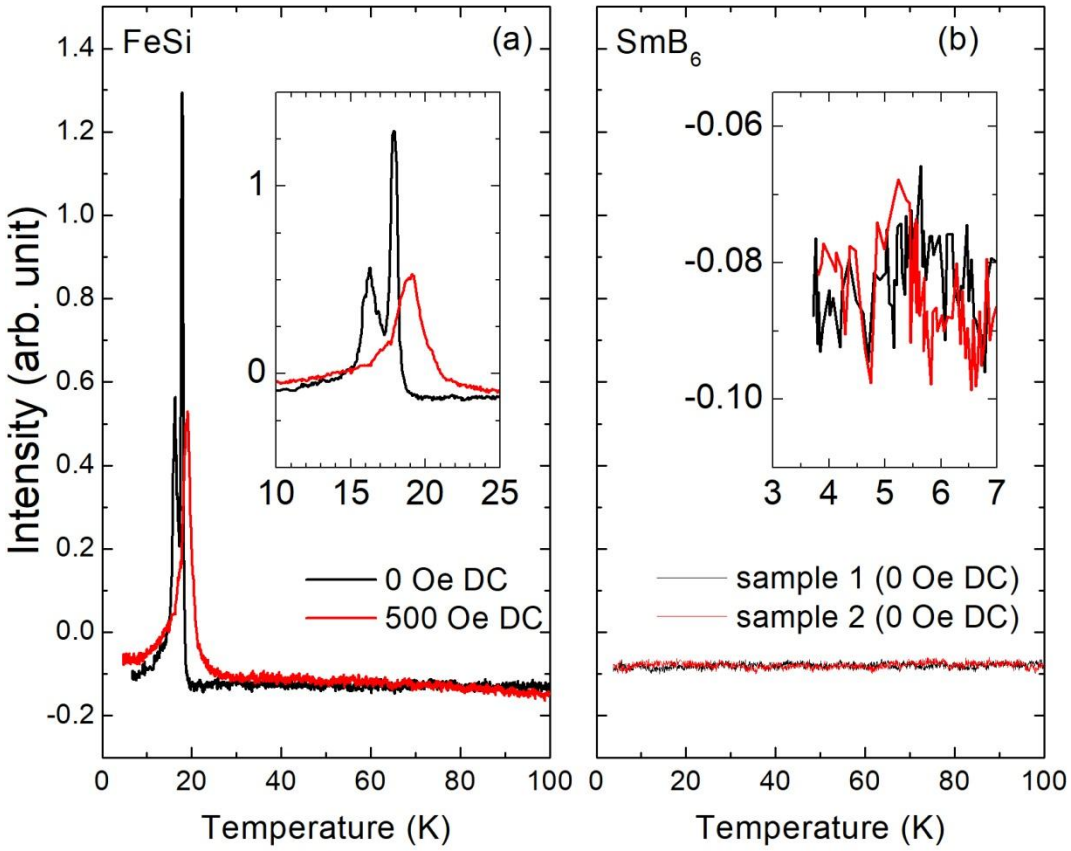


**Figure 5-8** Temperature dependence of the microwave absorption signal (MFMMS intensity) for both FeSi and $SmB_6$. (a)FeSi: The MFMMS signal for FeSi at 0 Oe (black) and 500 Oe (red) applied DC magnetic field. The intensity decreases with field and the onset temperature increases from 19 K at 0 Oe to 21 K at 500 Oe. (b) $SmB_6$: The MFMMS signal for two different $SmB_6$ samples in zero applied DC field. No peaks were observed for repeated measurements down to 4K.

Magnetoresistance measurements performed on $SmB_6$ samples show evidence of a transition at about 4.5 K, as can been in Figure 5-9 (b), similar to those shown in Chen *et al.* [8]. Based on the data for FeSi from Fang *et al.* [1], we see the same minimum in the magnetoresistance (see Figure 5-9 (a)). The field dependent data for the magnetoresistance MR at various temperatures are shown for $SmB_6$ in Figure 5-9 (d) taken from Chen *et al.* [8] and for FeSi in Figure 5-9 (c), based on the data shown in Figure 5-2. In both FeSi and $SmB_6$, there is a large temperature dependence of the MR (gray and pink regions) in Figure 5-9 (a), (b) around the respective Kondo Temperatures $T_K$. Similar behavior for FeSi and $SmB_6$ can also be seen in the

field dependence of the *MR* where below (above) $T_K$, there is a weak (strong) dependence of *MR* on field.

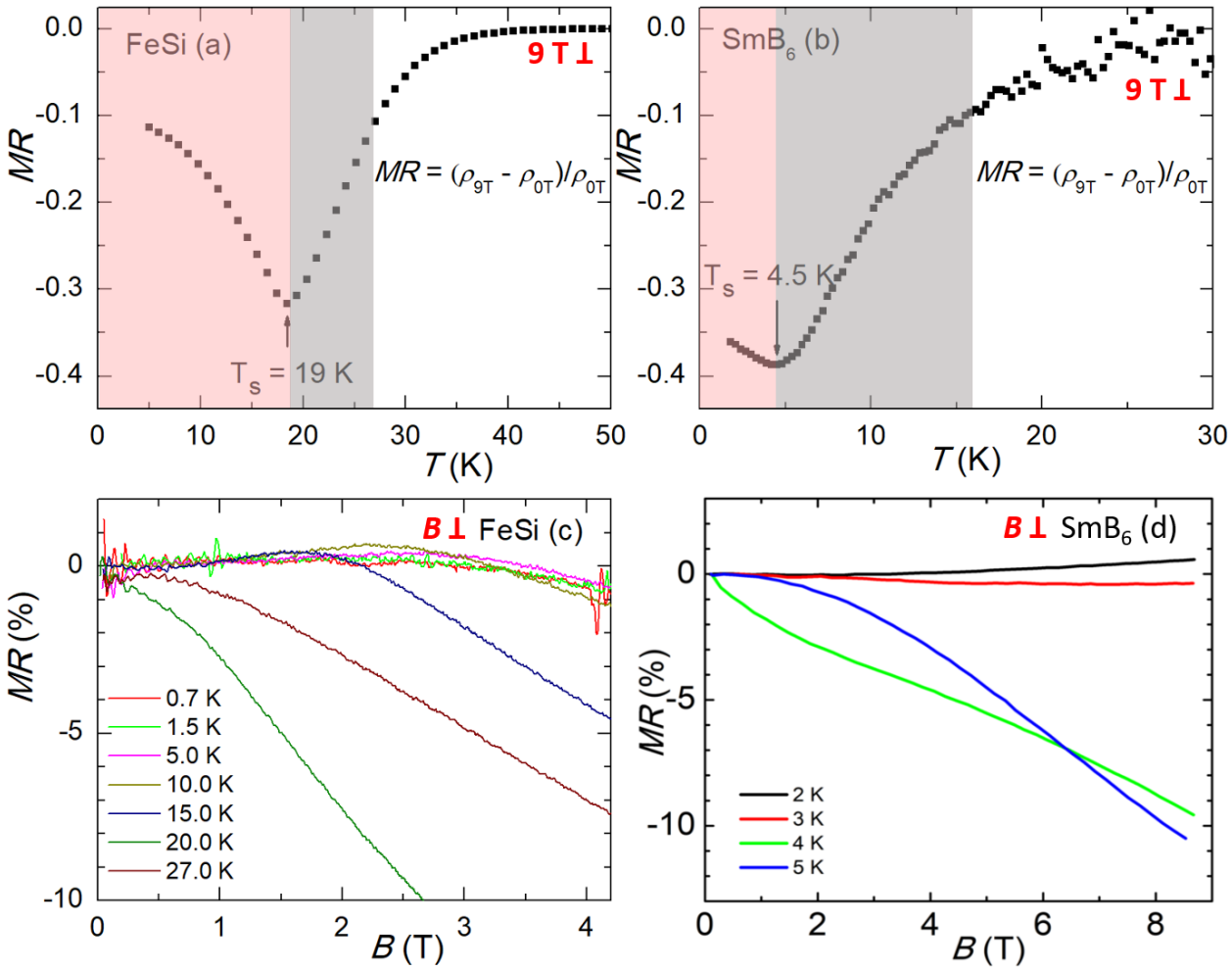


**Figure 5-9** Comparison of the magnetoresistance *MR* of FeSi and $SmB_6$ as a function of temperature T through $T_S$ at a magnetic field B = 9T [panels (a) and (b)] and as a function of B at various values of T below and above $T_S$ [panels (c) and (d)] The magnetoresistance is defined as $MR = [R(B) - R(0\ \mathrm{T})]/R(0\ \mathrm{T})$, where *B* is the applied external magnetic field. Data in panel (a) are from Fang *et al.* [1], in panel (b) from this work, in panel (c) from this work (data in Fig. 5-2), and panel (d) from Chen *et al.* [8].

A comparison of the electrical and magneto-transport properties suggests that both FeSi and $SmB_6$ behave as Kondo insulators, with evidence for the existence of a surface state and topological behavior. However, as a measure of the change to a particular sample's surface

resistivity, the MFMMS measurements of FeSi and $SmB_6$ suggest there are differences between these two samples with regard to their surface physics. Although most regard $SmB_6$ as a topological material [5, 20], there are competing interpretations [21, 22]. Further research will be required to determine why the MFMMS measurements are able to detect the onset of the conducting surface state in FeSi, but not $SmB_6$.

**Acknowledgements**

A. B., Y. D., C. M., Y. F., and M. B. M. would like to acknowledge funding from DOE BES DEFG02-04-ER46105 (materials synthesis, high pressure measurements) and NSF/DMR-1810310 (physical properties measurements). *$SmB_6$ synthesis*: P. F. S. R. and Z. F. acknowledge the funding from DOE 2019LANLE1FR. *High pressure transport by DAC*: Q. Z. acknowledges the financial support from NSFC (No. 51871054). The research performed by L. S. was supported by the National Key Research and Development Program of China (No. 2017YFA0303104 and No. 2016YFA0300503). Y. D. would like to thank Prof. P. Riseborough at the Temple University for the discussion about Kondo insulators under pressure. *High field transport*: J. S. acknowledges funding from NSF/DMR-1157490/1644779 and the State of Florida. *MFMMS*: C. T. W and I. S acknowledge funding from DOE BES grant No. DE FG02 87ER-45332.

Chapter 5, in full, is currently being prepared for submission for publication of the material. Deng, Yuhang; Moir, Camilla; Fang, Yuankan; Lou, Hongbo; Li, Shubin; Zeng, Qiaoshi; Shu, Lei; Wolowiec, Christian; Schuller, Ivan; Rosa, Priscila; Fisk, Zachary; Singleton, John; Maple, M. Brian. The dissertation author was the primary investigator and author of this material.

## Bibliography


1. Yuankan Fang, Sheng Ran, Weiwei Xie, Shen Wang, Ying Shirley Meng, and M. Brian Maple. "Evidence for a conducting surface ground state in high-quality single crystalline FeSi," *Proceedings of the National Academy of Sciences* **115**, 8558-8562 (2018), DOI: https://doi.org/10.1073/pnas.1806910115

2. S. Gabáni, Ernst Bauer, Stefan Berger, K Flachbart, Y Paderno, Ch Paul, V. Pavlík, and N. Shitsevalova. "Pressure-induced Fermi-liquid behavior in the Kondo insulator $SmB_6$: Possible transition through a quantum critical point," *Physical Review B* **67**, 172406 (2003), DOI: https://doi.org/10.1103/PhysRevB.67.172406

3. A. Sousanis, P. F. Smet, and D. Poelman. "Samarium monosulfide (SmS): Reviewing properties and applications," *Materials* **10**, 953 (2017), DOI: https://doi.org/10.3390/ma10080953

4. Maxim Dzero, Kai Sun, Victor Galitski, and Piers Coleman. "Topological Kondo insulators," *Physical Review Letters* **104**, 106408 (2010), DOI: https://doi.org/10.1103/PhysRevLett.104.106408

5. Maxim Dzero, Jing Xia, Victor Galitski, and Piers Coleman. "Topological Kondo insulators," *Annual Review of Condensed Matter Physics* **7,** 249-280 (2016), DOI: https://doi.org/10.1146/annurev-conmatphys-031214-014749

6. Yoichi Ando. "Topological insulator materials," *Journal of the Physical Society of Japan* **82**, 102001 (2013), DOI: https://doi.org/10.7566/JPSJ.82.102001

7. B. Tummers. Datathief III, (2006)

8. F. Chen, C. Shang, Z. Jin, D. Zhao, Y. P. Wu, Z. J. Xiang, Z. C. Xia, A. F. Wang, X. G. Luo, T. Wu, and X. H. Chen. "Magnetoresistance evidence of a surface state and a field-dependent insulating state in the Kondo insulator $SmB_6$," *Phys. Rev. B* **91**, 205133 (2015), DOI: https://doi.org/10.1103/PhysRevB.91.205133

9. Biao Yang, Martin Uphoff, Yi-Qi Zhang, Joachim Reichert, Ari Paavo Seitsonen, Andreas Bauer, Christian Pfleiderer, and Johannes V. Barth. "Atomistic investigation of surface characteristics and electronic features at high-purity FeSi(110) presenting interfacial metallicity," *Proceedings of the National Academy of Sciences* **118**, e2021203118 (2021), DOI: https://doi.org/10.1073/pnas.2021203118

10. A. Kebede, M. C. Aronson, C. M. Buford, P. C. Canfield, Jin Hyung Cho, B. R. Coles, J. C. Cooley, J. Y. Coulter, Z. Fisk, J. D. Goettee, W. L. Hults, A. Lacerda, T. D. McLendon, P. Tiwari, and J. L. Smith. "Studies of the correlated electron system $SmB_6$," *Physica B: Condensed Matter* **223&224**, 256 - 259 (1996), DOI: https://doi.org/10.1016/0921-4526(96)00092-0

11. Yuhang Deng and J. S. Schilling. “Enhanced magnetic ordering in Sm metal under extreme pressure,” *Physical Review B* **99**, 085137 (2019), DOI: https://doi.org/10.1103/PhysRevB.99.085137

12. Christian Pfleiderer. “Superconducting phases of *f*-electron compounds,” *Reviews of Modern Physics* **81**, 1551 (2009), DOI: https://doi.org/10.1103/RevModPhys.81.1551

13. Juan Gabriel Ramírez, Ali C Basaran, J. de la Venta, Juan Pereiro, and Ivan K Schuller. “Magnetic field modulated microwave spectroscopy across phase transitions and the search for new superconductors,” *Reports on Progress in Physics* **77**, 093902 (2014), DOI: https://doi.org/10.1088/0034-4885/77/9/093902

14. Jung-Fu Lin, Andrew J Campbell, Dion L Heinz, and Guoyin Shen. “Static compression of iron-silicon alloys: Implications for silicon in the earth’s core,” *Journal of Geophysical Research: Solid Earth* **108**, 2045 (2003), DOI: https://doi.org/10.1029/2002JB001978

15. Rebecca A. Fischer, Andrew J. Campbell, Daniel M. Reaman, Noah A. Miller, Dion L. Heinz, Przymyslaw Dera, and Vitali B. Prakapenka. “Phase relations in the Fe-FeSi system at high pressures and temperatures,” Earth and Planetary Science Letters **373**, 54-64 (2013), DOI: https://doi.org/10.1016/j.epsl.2013.04.035

16. E. Bauer, S. Bocelli, R. Hauser, F. Marabelli, and R. Spolenak. “Stoichiometric effects on the optical spectra and pressure response of $Fe_{1-x}Mn_xSi$,” *PhysicaB: Condensed Matter* **230**, 794-796 (1997), DOI: https://doi.org/10.1016/S0921-4526(96)00842-3

17. J. Beille, M. B. Maple, J. Wittig, Z. Fisk, and L. E. DeLong. “Suppression of the energy gap in $SmB_6$ under pressure,” *Physical Review B* **28**, 7397 (1983), DOI: https://doi.org/10.1103/PhysRevB.28.7397

18. J. C. Cooley, M. C. Aronson, Z. Fisk, and P. C. Canfield. “$SmB_6$: Kondo insulator or exotic metal?” *Physical Review Letters*, **74**, 1629 (1995), DOI: https://doi.org/10.1103/PhysRevLett.74.1629

19. Daniel J. Campbell, Zachary E. Brubaker, Connor Roncaioli, Prathum Saraf, Yuming Xiao, Paul Chow, Curtis Kenney-Benson, Dmitry Popov, Rena J. Zieve, Jason R. Jeffries, and Johnpierre Paglione. “Pressure-driven valence increase and metallization in the Kondo insulator $Ce_3Bi_4Pt_3$,” *Physical Review B* **100**, 235133 (2019), DOI: https://doi.org/10.1103/PhysRevB.100.235133

20. G. Li, Z. Xiang, F. Yu, T. Asaba, B. Lawson, P. Cai, C. Tinsman, A. Berkley, S. Wolgast, Y. S. Eo, Dae-Jeong Kim, C. Kurdak, J. W. Allen, K. Sun, X. H. Chen, Y. Y. Wang, Z. Fisk, and Lu Li. “Two-dimensional Fermi surfaces in Kondo insulator $SmB_6$,” *Science* **346**, 1208-1212 (2014), DOI: https://doi.org/10.1126/science.1250366

21. P. Hlawenka, K. Siemensmeyer, E. Weschke, A. Varykhalov, J. Sánchez-Barriga, N. Y. Shitsevalova, A. V. Dukhnenko, V. B. Filipov, S. Gabáni, K. Flachbart, O. Rader, and E.

D. L. Rienks. “Samarium hexaboride is a trivial surface conductor,” *Nature Communications* **9**, 517 (2018), DOI: https://doi.org/10.1038/s41467-018-02908-7

22. S. M. Thomas, Xiaxin Ding, F. Ronning, V. Zapf, J. D. Thompson, Z. Fisk, J. Xia, and P. F. S. Rosa. “Quantum oscillations in flux-grown $SmB_6$ with embedded aluminum,” *Phys. Rev. Lett.* **122**, 166401 (2019), DOI: https://doi.org/10.1103/PhysRevLett.122.166401